AD-A141 112 FAILURE BY CREEP CRACKING AND CREEP FATIGUE INTERACTION IN NICKEL BASE SU..(U) CORNELL UNIV ITHACA NY DEPT OF MATERIALS SCIENCE AND ENGINEER.. R RAJ JAN 84 1/1

UNCLASSIFIED AFOSR-TR-84-0339 AFOSR-80-0008 F/G 11/6 NL

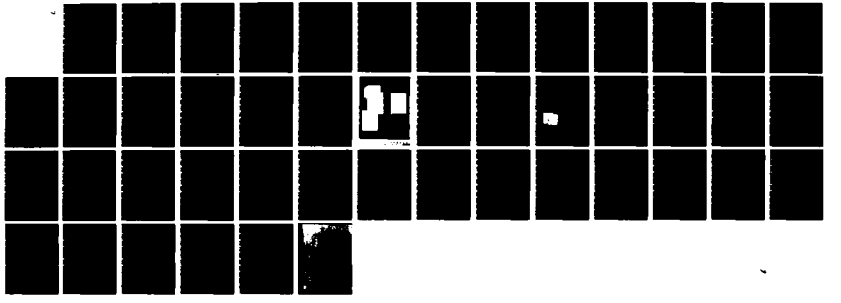

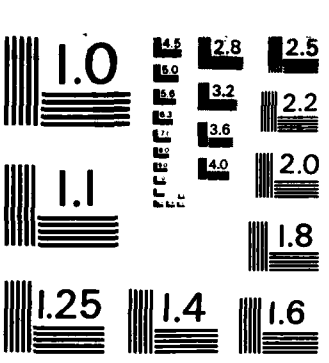

MICROCOPY RESOLUTION TEST CHART
NATIONAL BUREAU OF STANDARDS - 1963 - A

Final Technical Report

to

Air Force Office of Scientific Research

(Project Manager: Dr. A.H. Rosenstein)

Grant No.: AFOSR-80-0008

FAILURE BY CREEP CRACKING AND CREEP FATIGUE INTERACTION IN NICKEL BASE SUPERALLOYS

Principal Investigator

Rishi Raj

Professor

Department of Materials Science and Engineering

Cornell University

Ithaca, New York 14853

January 1984

CONTENTS

SUMMARY

Most high temperature structural materials exhibit a minimum in ductility near one half of their melting point. The embrittlement occurs by the nucleation and growth of cavities in the grain boundaries. The objective of this investigation was to study the phenomenon of cavitation under conditions of creep-fatigue interaction and under creep crack growth. The first involved identifying and modeling the mechanisms by which cavitation may interact with the classical stage I and stage II crack growth in low cycle fatigue. Creep crack growth involved the growth of cavities in the local stress and strain field of a crack tip.

In the creep-fatigue work, experiments were carried out on model materials to identify various mechanisms of failure. At least five were found. The dominant one depended on the cycle shape, the frequency, temperature and the microstructure of the material. Cavitation was found to accelerate the initiation and propagation of fatigue cracks; these were the cases where creep damage interacted with the cracks which are normally produced under condition of low cycle fatigue. In other instances cyclic loading served to enhance cavitation damage; in this case failure occurred by the gradual accumulation of cavitation damage throughout the specimen rather than by the initiation and growth of a fatigue crack. The cavitation mode of failure was theoretically analyzed.

The accepted mechanism of creep crack growth is the nucleation and growth of cavities in the local stress field of the crack tip. Experiments were carried out on the nickel base superalloy MERL 76, to study the influence of loading rate on creep crack growth in compact tension specimens. We found that a slower loading rate decreased the fracture toughness. The result was explained in terms of the relative magnitude of plastic flow and the growth of

cavitation damage in front of the crack tip. It was argued that if the loading conditions favored damage rather than plastic flow, then the toughness will be lowered. Local plastic strain and damage strain near the crack tip were measured by the distortion of a lattice of markers etched on the specimen surface (using photo-lithography techniques). The lower fracture toughness was found to be associated with a higher value of damage strain relative to the plastic strain. A theoretical model was developed to describe the results. The model is general and may be used to predict creep crack growth behavior.

The grant provided whole or primary support for one post-doctoral associate, two Ph.D. students and one M.S. student. Eight papers have been published in Metallurgical Transactions, Acta Metallurgica and Metal Science, and one more has been accepted for publication in Acta Metallurgica.

INTRODUCTION

Grain boundaries have been recognized as planes of weakness in structural materials developed for high temperature applications. The embrittlement occurs at about the temperatures used in service. With the development of superalloys which have outstanding creep strength, fracture rather than creep behavior has become the more important consideration in design.

The mechanism of failure at elevated temperatures has been recognized to be the nucleation and growth of sub-micron cavities in grain interfaces. The cavities prefer to form at second phase particles such as the carbides and sometimes the gamma-prime precipitates [1,2]. The spacing of the cavities, therefore, is of the same order as the spacing of the precipita The closer this spacing the smaller is the ductility of the material. The ease of cavity nucleation also plays an important role in the determination of time to failure. It has been hypothesized that the environmental sensitivity of nickel base superalloys may be tied to the nucleation of cavities. One idea is that oxygen diffuses from the surface along the grain boundaries, reacts with the carbides to produce molecules of CO gas which promote the nucleation of cavities [3]. The oxidation of the carbide-matrix interface also weakens the boundary since oxides are generally less securely bonded to the matrix than the carbides [4].

The objective of this investigation was to study the mechanisms of failure under conditions of creep-fatigue interaction, and creep-crack-growth. The approach was to identify the mechanisms and then develop models for describing failure in terms of the loading variables and the microstructure. In the following sections, the results from each topic are summarized. Further details of the work are available in publications.

In addition to the work related directly to creep-fatigue and creep-crack growth, additional papers on cavitation were also published in the course of this investigation, notably on intergranular fracture under aggressive environments and on the description of damage under multiaxial loading. These papers will not be discussed in this report, but are attached in the Appendix.

CREEP CRACK GROWTH

The principal difference between stress-rupture, in smooth specimens, and creep-crack-growth, in notched specimens is that in notched specimens the nucleation and growth of cavities is limited to the crack-tip region. In fact the crack grows because the cavities coalesce ahead of the crack tip. A picture of such a mechanism is shown in Fig. 1. The modeling of such a process is complicated by the following factors:

(a) The stress field near the crack-tip is non-uniform, multiaxial, and time dependent.

(b) The nucleation and growth of cavities is time dependent even under a constant stress. Since the stress also varies with time the cavitation behavior can be analyzed only after making simplifying assumptions.

(c) Growth of cavities produces dilation in the material. This can alter the stress in the crack-tip region.

(d) Since the cavities form near the surface, environmental effects may play an important role in creep crack growth.

In the present research program we have completed three tasks. First a simple model for creep crack growth has been analyzed. In the model we have assumed that the cavities grow by diffusion and that the stress field in front of the crack is determined by the coupling between elastic deformation and time dependent cavity growth. In the second task we have examined the influence of the rate of loading on fracture toughness in MERL'76 at 1000K (1340°F). We have found that fracture toughness increases with increasing rate of loading. The result was explained in terms of the relative magnitude of plastic-strain and (cavitation) damage-strain near the crack-tip. It was argued that plastic flow and cavitation compete for dominance near the crack-tip. At slower

loading-rates, cavitation is dominant and the fracture toughness is low. Thirdly, we have developed a simple numerical model for creep crack growth where plastic flow as well as cavitation contribute to strain in the crack-tip region. The results of the model are in good agreement with experiments on MERL'76. The results from each of these tasks are now described.

Crack Growth Model - I

The growth of cavities in grain boundaries stressed in uniform tension, has been examined in detail in the literature [5-8]. The physical mechanism of cavity growth is illustrated in Fig. 2. Cavities grow by the transfer of atoms from cavity surfaces to the grain interface. As a result the cavities grow in size and the matter "plated" onto the grain boundary is accomodated by rigid body displacement of the two half crystals. If the cavities are assumed to have an equilibrium shape, then the grain boundary damage, A_r, defined as the separated fraction of the boundary area, the normal displacement of the crystals, u, and the average cavity spacing, λ, are related to each other by geometry. The detailed expressions are given in Ref. 9. If we normalize u with respect to λ, so that:

$$\bar{u} = \frac{u}{\lambda} \tag{1}$$

then the rate of growth of cavities (expressed in terms of u) can be related to the (normalized) applied stress, $\bar{\sigma}_0$ by:

$$\frac{d\bar{u}}{d\bar{t}} = (\bar{\sigma}_0 - \bar{\sigma}^*) \tag{2}$$

In (2), $\bar{\sigma}^*$ is the threshold stress for the nucleation of cavities and $\bar{t}$ is a normalized unit of time which depends on temperature through the boundary diffusion coefficient. The stress in equation (2) has been normalized with respect to the Young's Modulus. Equation (2) is the simple rather than the

exact version of the growth equation. The latter is discussed in Ref. 9.

Recalling that the damage, A_r is related to $\bar{u}$ through geometry, the fracture conditon, defined as the point where neighbor cavities grow to touch each other, can be defined in terms of $\bar{u}$. It may be shown that this critical displacement, $u_c = 0.4$.

The stress field near a crack-tip is non-uniform and the displacement required to accomodate cavity growth will generate elastic back stresses, which will tend to relax the stress field at the crack-tip. That is the problem which we have analyzed in detail. One set of results are shown in Figure 3. Growth of cavities, which is characterized by the displacement u, relaxes the stress field. When $u = u_c$ at the crack-tip, the crack advances by one unit spacing. The calculation leads to the following interesting results:

(i) Crack velocity reaches a steady state after a readjustment of the stress field near the crack-tip.

(ii) For a crack moving in the steady state, the stress field remains constant.

(iii) The steady state crack-velocity, $\dot{a}$, is proportional to K_I^2, where K_I is the applied stress-intensity factor.

(iv) A characteristic damage zone, of size Z_A, develops in front of the crack-tip. Z_A also depends on K_I.

(v) Crack will not propagate if $K_I < K_{th}$. The threshold is related to the threshold stress for cavity nucleation.

The equations for the above properties of the model are given below:

$$K_{th} = (0.4\ \lambda E \sigma^*)^{1/2} \tag{3}$$

$$\dot{a} = 7\times10^{5}\,\frac{K_I^2\Omega}{EkT}\,\frac{\delta D_b}{\lambda^3} \quad \text{when } K_I > K_{th} \tag{4a}$$

$$\dot{a} = 0 \quad \text{when } K_I \leq K_{th} \tag{4b}$$

In equations (3) and (4), E is the Young's modulus and Ω is the atomic volume. Although the equations agree quite with experiment in threshold behavior and K_I^2 dependence of crack-velocity, the measured crack velocities [10,11] appear to be about two to three orders of magnitude slower than those calculated. The discrepancy may arise from (i) the assumption that the crack moves in a flat plane rather than in a zig-zag manner as would be the case for an intergranular path in a polycrystal and, (ii) the influence of plastic flow, which has been disregarded in the model, on the crack-tip stress field. A comparison between theory and experiment is given in Ref. 9.

Experiments to Measure Fracture Toughness of MERL'76 at 1000K

We have measured fracture toughness as the work of fracture required to initiate and propagate an intergranular crack from a notch in compact-tension-specimens. The concept underlying the experiments is illustrated in Fig. 4(a) and (b). Deformation near the crack-tip has two components: plastic flow, and grain boundary cavitation damage. Plasticity concentrates along the shear lobes where the shear stress is maximum. Cavitation, on the other hand would localize immediate ahead of the crack-tip since it responds to the maximum tensile stress. Whereas plastic flow will blunt the crack-tip, cavitation will move the crack forward and keep it sharp. Our view was that the relative magnitude of plastic strain and damage strain would influence the measured fracture toughness of the material. Their relative magnitude could be changed through the loading rate. We expected that the slower loading rates would enhance the relative significance of damage and, therefore, lower the fracture toughness.

The experimental results shown in Fig. 4(d) are in agreement with the above hypothesis. In order to confirm the hypothesis, the damage strain and the plastic strain were measured directly. The technique was to etch markers on the surface at a spacing of 6μm. Plastic strain was defined as the deformation of the grains, and was measured as the distortion of the etched grid on the scale of one grain size. Cavitation strain was defined, and measured, as the average separation of the grain interfaces per unit distance. A picture of a situation where the damage strain is significant but the plastic strain is negligible is shown in Fig. 4(c). A plot of the ratio of the plastic strain to damage strain is given in Fig. 4(d); note that the increase in the fracture toughness is directly correlated to this ratio.

An approximate computer analysis was developed to describe the results by a quantitative model. The model has been described quantitatively in Ref.12. The details of the model will not be discussed here. The results of the model were in good agreement with experiment as illustrated in Fig. 4(d).

CREEP-FATIGUE INTERACTION

Experiments

Creep-fracture is characterized by the nucleation and growth of cavities at grain boundaries, while low-cycle-fatigue is characterized by the Stage I crack initiation and Stage II propagation of a transgranular crack. Separately both failure processes are well understood but the interactions between them appear to be complex. A linear damage rule which assumes that the fatigue portion (defined by the number of cycles) and creep portion (defined as the time spent at maximum stress) add to cause failure has proved to be too simplistic. The data when plotted by this rule show a very large scatter suggesting that the interaction mechanisms are non-linear and that more than one type of interactions may be possible.

Our approach to the above dilemma was to carry out systematic experiments to characterize the mechanisms of creep-fatigue interactions. Aluminum-five percent magnesium alloy was chosen for the study because it has been shown to be very resistant to intergranular creep-fracture under monotonic loading. Experiments were done on smooth specimens with a uniform gage section (as opposed to hour-glass shaped specimens) and in ultra-high-vacuum to reduce the effects of the environment to a minimum. The temperature and the cycle shape were varied, but the plastic strain size and the frequency were held constant. It was felt that frequency and temperature are complementary parameters which may be normalized with respect to each other.

The results of the experiments are shown in Fig. 5b. The cycle shapes which were used are drawn in Fig. 5a. Metallography and fractography revealed at least five different failure mechanisms of creep fatigue interaction. They are designated by (a) thru (e) in Fig. 5b. Each one is described below. Further details and the micrographs are contained in Ref. 13.

(a) This was the classical low-cycle-fatigue mode of failure which is produced by the transgranular initiation of a Stage I crack and propagation of a Stage II transgranular crack. The propagation is characterized by striations on the fracture surface. The spacing of the striations is believed to be related to the crack-tip-opening-displacement [14].

(b) This failure mode occurred for all three cycle shapes at 423K, and at 473K for the equal ramp cycle shape. It differed from (a) in that crack-initiation changed transgranular to intergranular. But propagation remained transgranular and was marked by striations.

(c) This failure mode dominated at higher temperatures when the cycle shape contained a tensile hold-time. In this case the failure mode was totally different. Instead of crack initiation and propagation, intergranular creep damage was spread throughout the specimen. Interrupted tests under the same conditions revealed that the damage accumulated gradually with fatigue cycles. The damage was of 'r' type of cavities as shown schematically in Fig. 6.

(d) In this case, as in (c), failure was caused by cumulative creep damage, the difference being that 'wedge' type of grain boundary cracks were formed. The difference between 'r' and 'wedge' cavities is illustrated in Fig. 6. The cumulative nature of the damage, which was spread throughout the specimen, was confirmed through interrupted tests.

(e) Here a macroscopic instability and flow localization developed in the gage length of the specimen. It is possible that the instability was caused by microstructural degradation of magnesium-aluminide precipitates at 573K.

Theory

The cumulative damage mechanism of creep-fatigue interaction for the 'wedge' type of intergranular cavities was formulated and analyzed in detail.

This is the type (d) failure described in the previous seciton. The physical basis of the analysis and the cogent results are described here. The details are given in Ref. 15.

The crucial role of grain boundary sliding in the growth of wedge cracks may be appreciated from the schematic in Fig. 6(a). The basis of the model then is to correlate the applied strain to the local sliding at grain boundaries, and the sliding to the wedge crack damage. First, wedge damage, A_w, is defined by the equation:

$$A_w = \frac{w}{L} \tag{5}$$

where w is the length of the wedge crack and L is the grain size. The sliding displacement, v, at the triple junction where the wedge crack initiates is also normalized with respect to the grain size, so that at:

$$v = \frac{v_{sliding}}{L} \tag{6}$$

Then a simplifying assumption is made that A_w and v are linearly related through a material parameter, α:

$$\frac{dA_w}{dv} = \alpha \tag{7}$$

The connection between the applied strain ε_e and the sliding strain, v, is complex but has been extensively studied experimentally and theoretically. Defining a quality β such that:

$$\beta = \frac{v}{\varepsilon_e} \tag{8}$$

it may be shown that β varies sigmoidally with strain-rate as shown in Fig. 7. At slow strain rates β approaches 0.5. As the strain-rate increases there is a transition until sliding becomes zero at very high strain-rate. The important

parameter is the strain-rate at which the transition is felt. It, $\dot{\varepsilon}_w^*$, is a material parameter and has been found to depend on the microstructure of the grain boundary by the following equation:

$$\dot{\varepsilon}_w^* = \frac{0.27Y\Omega}{kT} \frac{\delta D_b}{f_b p^2 L} \tag{9}$$

Here Y is the yield stress, p is the size of the particles in the boundary and f_b is the area fraction of the particles in the boundary. In cases where these parameters cannot be characterized we have shown that $\dot{\varepsilon}_w^*$ may be experimentally measured with the use of internal friction measurements of grain boundary sliding rate. These details are discused in Refs. 13 and 17.

Equations (7) and (8), when combined give the result that:

$$\frac{dA_w}{d\varepsilon_e} = \alpha \tag{10}$$

where $\beta = \beta(\dot{\varepsilon}_e/\dot{\varepsilon}_w^*)$.

For a slow-fast cycle shape, the value of β in the tensile half of the cycle will be greater than in the compressive half of the cycle, because the tensile strain-rate is slower. If the tension strain-rate is $\dot{\varepsilon}_t$, and the compression strain-rate is $\dot{\varepsilon}_c$, then the damage per cycle will be given by:

$$\frac{A_\phi}{\Delta\varepsilon_p} = \alpha\beta(\dot{\varepsilon}_t) - \gamma\alpha\beta(\dot{\varepsilon}_c) \tag{11}$$

The first term in (11) is the positive damage caused by the tensile portion of the cycle. The second term is negative because compression would tend to heal the damage produced in tension. The coefficient γ has been asserted to account for the hysteresis in the recovery of damage. The cycles to failure, $N_f = 1/A_\phi$, which leads to the result:

$$\Delta\varepsilon_p N_f = \frac{1}{\alpha\{\beta(\dot{\varepsilon}_t) - \beta(\dot{\varepsilon}_e)\}} \tag{12}$$

The result in (12) shows that $N_f \propto 1/\Delta\varepsilon_p$ when cumulative creep damage is the mechanism of failure (in low-cycle-fatigue, Coffin-Manson equation predicts a parabolic power-law-dependence). Equation (12) does contain two adjustable parameters α and γ which can be fixed by simple experiments.

The application of the above result to our own measurements on aluminum and to published data for austentic stainless steels has been discussed in Ref. 15. The agreement is quite good. The application of the analysis to nickel base superalloys has been less successful suggesting that cumulative creep damage may not be the primary failure mode in superalloys at temperatures encountered by disks in gas-turbine engines. We believe that the intergranular crack initiation mechanism (described by (b) in Fig. 5b) is more relevant in nickel-base superalloys. The sensitivity of superalloys to oxygen environments could also complicate the prediction of life by the simple analysis as described in this report.

REFERENCES

1. B.F. Dyson, M.S. Loveday and M.F. Rodgers, Proc. R. Src. Lond., A349, 245 (1976).
2. K. Hiozawa and J.R. Weertman, Acta Metall., 31 [7], 993-1004 (1983).
3. D.A. Woodford, Metall. Trans., 12A, 299-308 (1981).
4. R. Raj, Acta Metall., 30, 1259-68 (1982).
5. D. Hull and D.E. Rimmer, Phil. Mag., 4, 653 (1959).
6. M.V. Speight and J.E. Harris, Metal Sci. J., 1, 83 (1967).
7. R. Raj and M.F. Ashby, Acta Metall., 23, 653 (1975).
8. R. Raj, H.M. Shih and H.H. Johnson, Scripta Metall., 11 839 (1977).
9. R. Raj and S. Baik, Metal Sci., 14, 385-94 (1980).
10. K. Sadananda and P. Shahinian, Metall. Trans., 8A, 439 (2977).
11. K. Sadananda and P. Shahinian, ibid., 9A, 79 (1978).
12. "Failure by Creep Cracking and Creep-Fatigue Interaction in Nickel Base Superalloys", Annual Tech. Report No.: 4, AFOSR-80-0008, April 1983, Department of Materials Science and Engineering, Cornell University, Ithaca, NY.
13. S. Baik and R. Raj, Metall. Trans., 13A [7], 1215-1221 (1982).
14. B. Tomkins, J. Engin. Mater. Tech., 97 [4], 298-97 (1975).
15. S. Baik and R. Raj, Metall. Trans., 13A [7], 1207-14 (1982).
16. F.W. Crossman and M.F. Ashby, Acta Metall., 23, 425 (1975).
17. C. Gandhi and R. Raj, Metall. Trans., 12A, 515-20 (1981).

FIGURE CAPTIONS

1. Cavities forming ahead of a crack-tip of an advancing creep crack in MERL'76 at 1000K.

2. The diffusional transport mechanism of cavity growth. Atoms are removed from the cavity surface and inserted into the grain boundary adjacent to the cavities.

3. Numerical results from Ref. 9, showing the relaxation of stress just ahead of the crack tip with the growth of cavities. U is a measure of cavity growth. Eventually the crack moves at a steady state.

4. Model, theory and experiment for the fracture toughness of MERL'76 at 1000K. Details given on page 8.

5. (a) The cycle shapes employed in experiments to identify the mechanisms of creep-fatigue-interaction. (b) The influence of cycle-shape and temperature on fatigue life and on the failure mechanism; five failure mechanisms were identified. Taken from Ref. 13.

6. A schematic of two types of creep damage.

7. Variation of the ratio, β, of strain due to sliding to the applied strain as a function of the applied strain-rate $\dot{\varepsilon}_e$ [16].

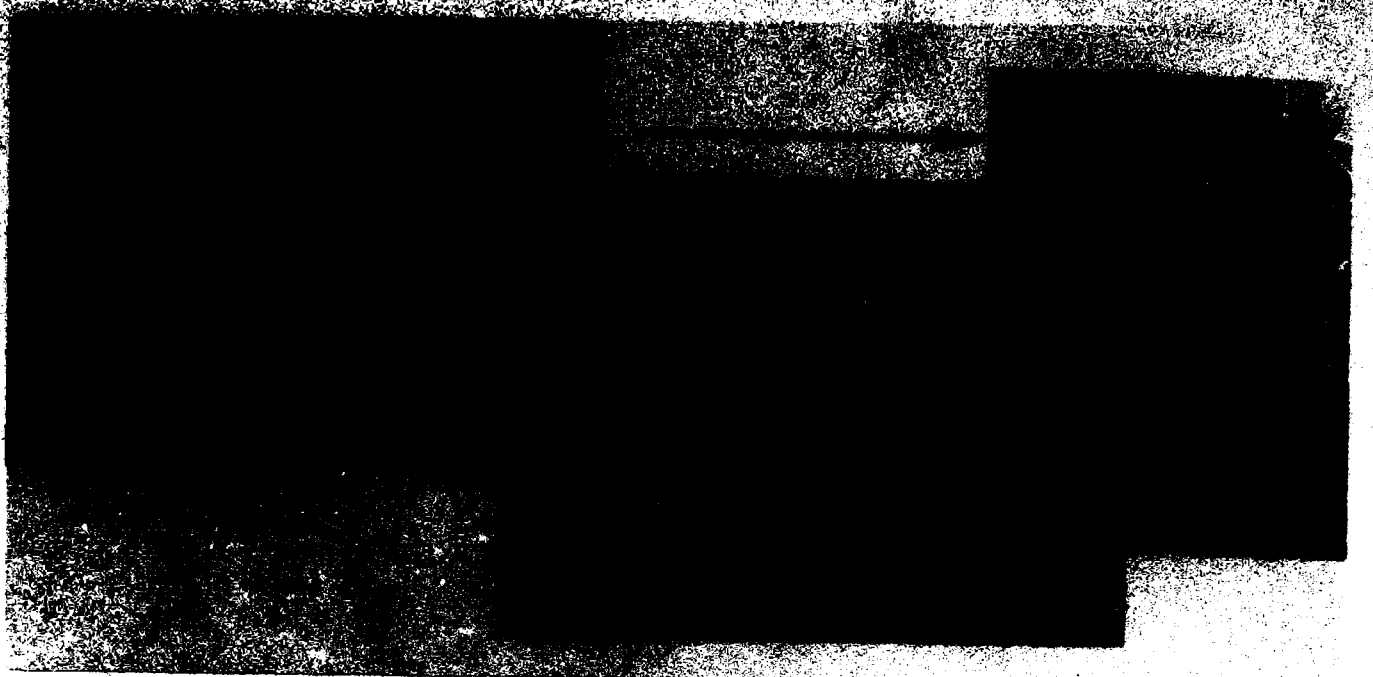

1. Cavities forming ahead of a crack-tip of an advancing creep crack in MERL'76 at 1000K.

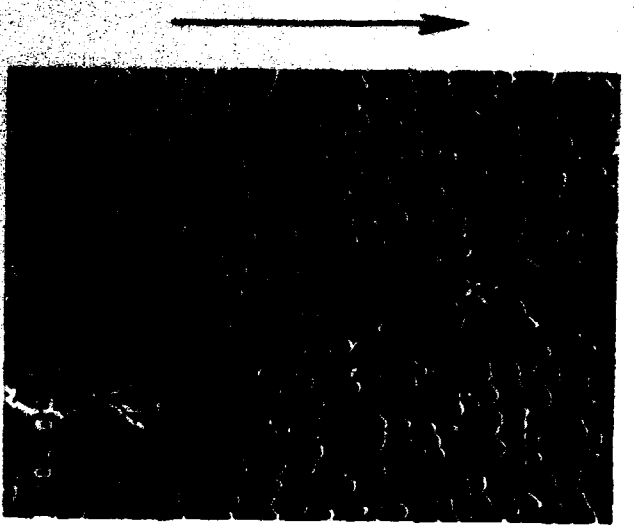

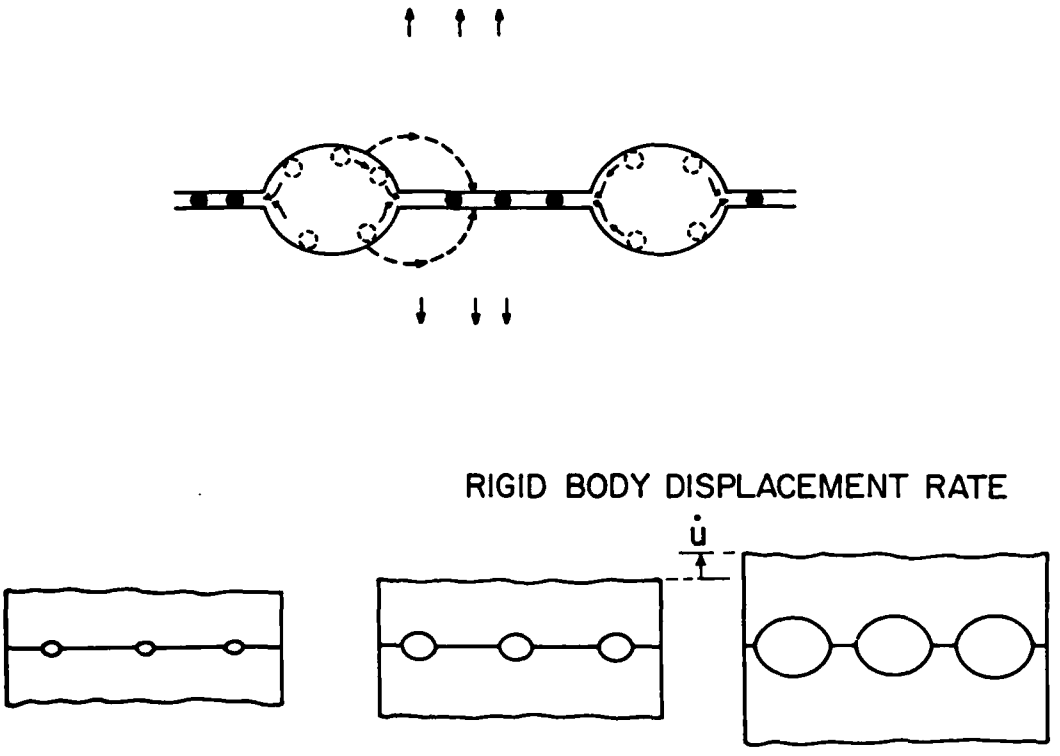

2. The diffusional transport mechanism of cavity growth. Atoms are removed from the cavity surface and inserted into the grain boundary adjacent to the cavities.

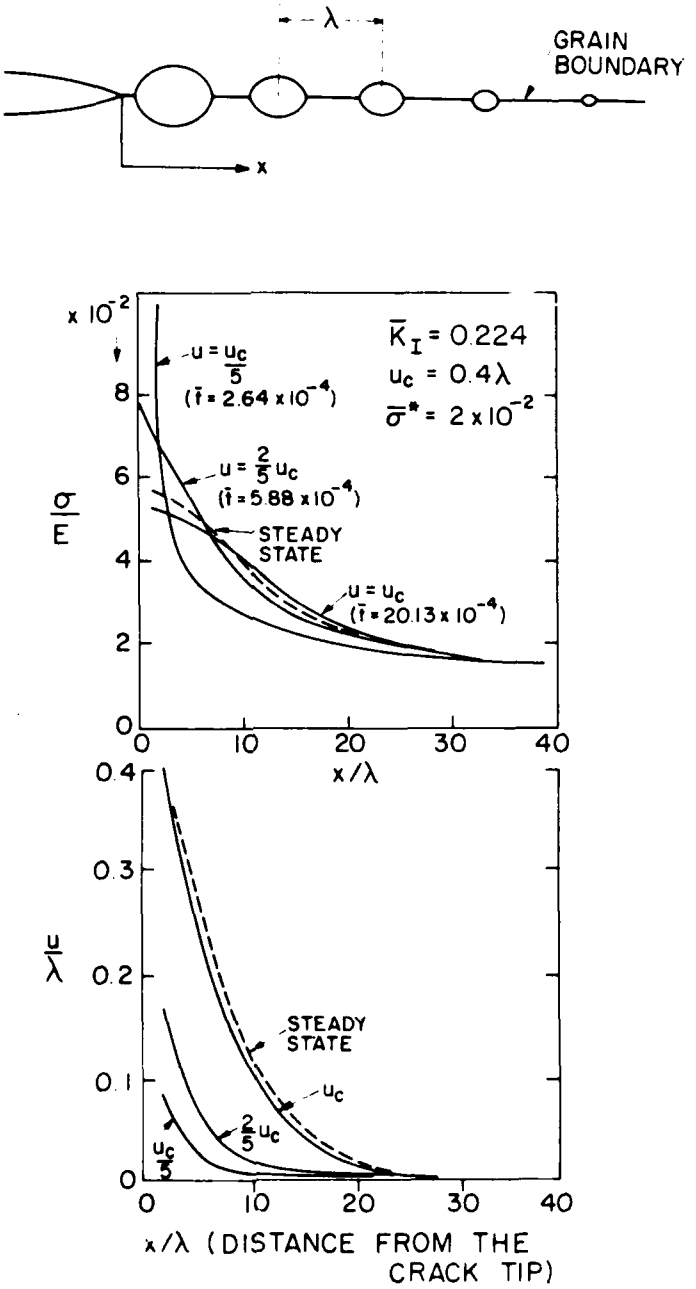

3. Numerical results from Ref. 9, showing the relaxation of stress just ahead of the crack tip with the growth of cavities. U is a measure of cavity growth. Eventually the crack moves at a steady state.

MODELING OF THE CREEP CRACK GROWTH PROCESS

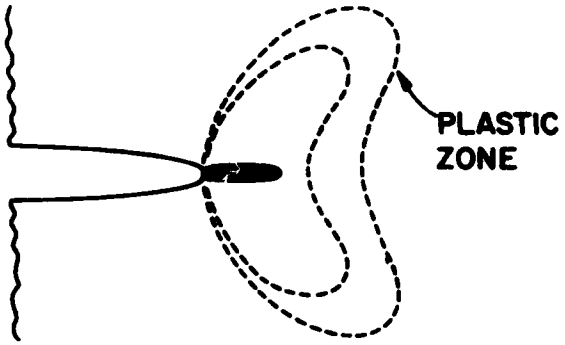

(a) HIGH TOUGHNESS

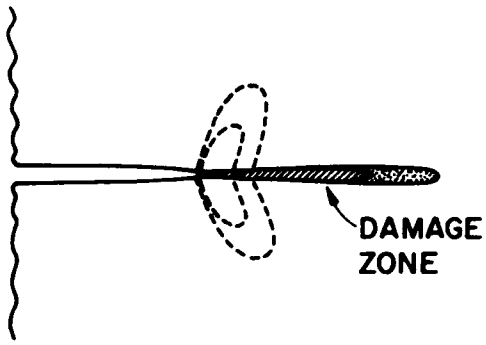

(b) LOW TOUGHNESS

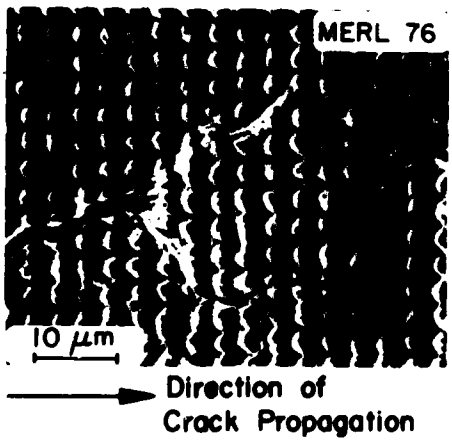

(c) DAMAGE DOMINATED DEFORMATION

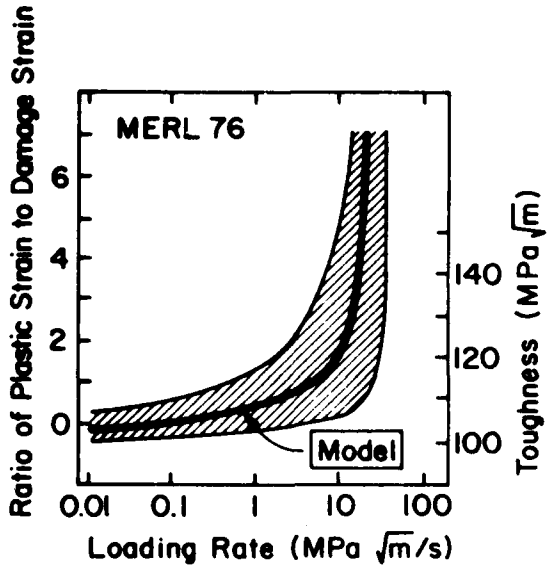

(d) INFLUENCE OF LOADING RATE ON DAMAGE

4. Model, theory and experiment for the fracture toughness of MERL'76 at 1000K. Details given on page 8.

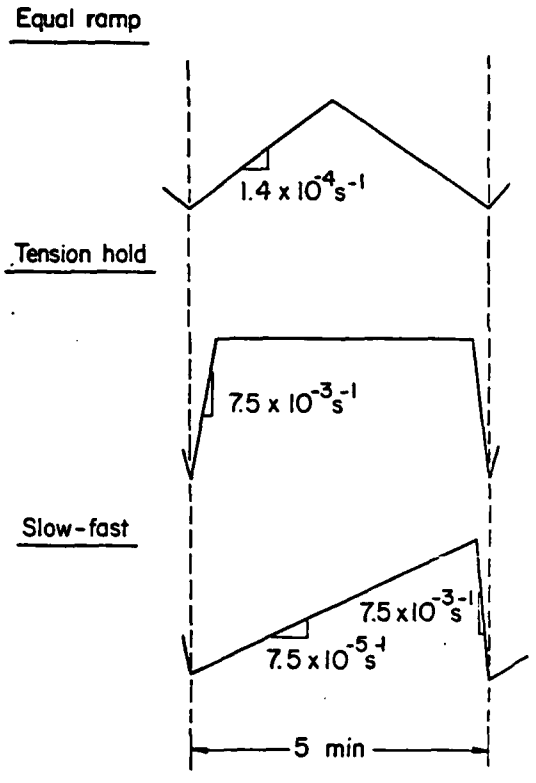

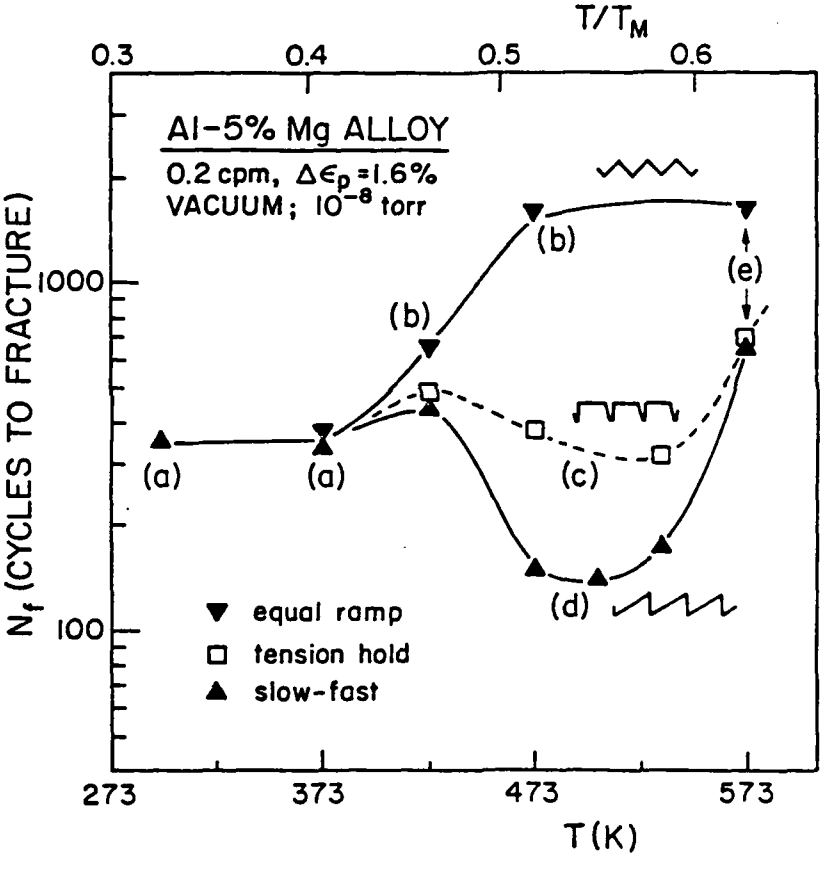

5. (a) The cycle shapes employed in experiments to identify the mechanisms of creep-fatigue-interaction. (b) The influence of cycle-shape and temperature on fatigue life and on the failure mechanism; five failure mechanisms were identified. Taken from Ref. 13.

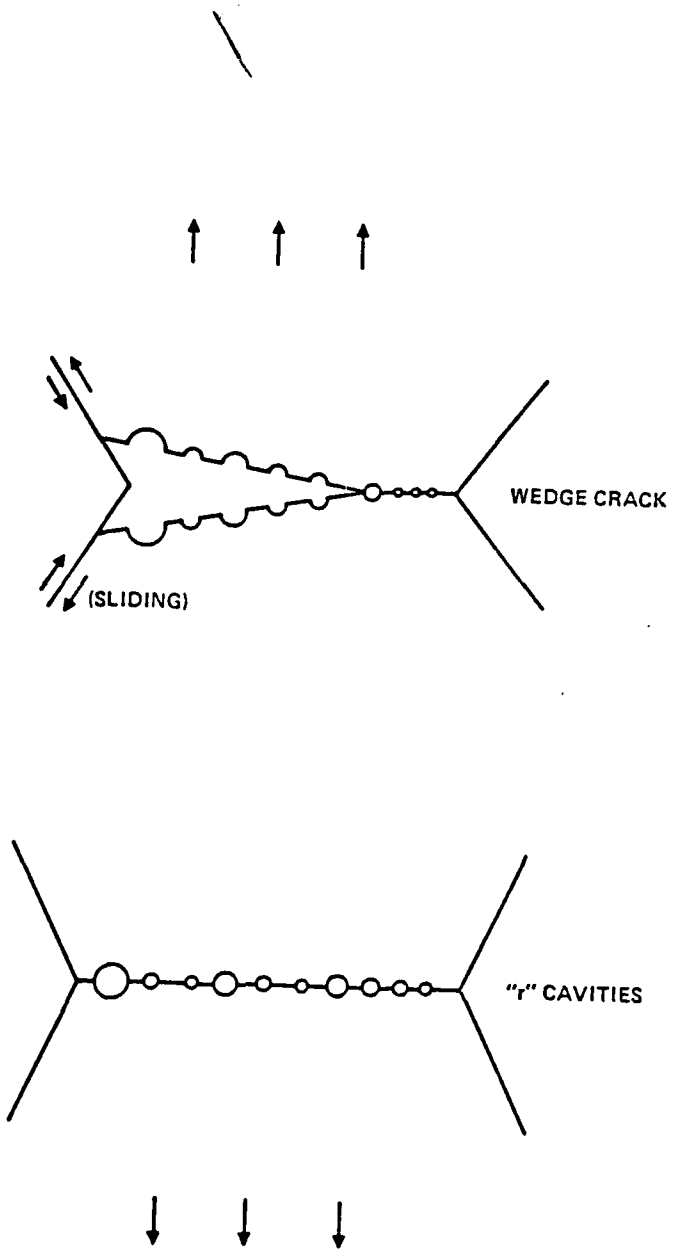

6. A schematic of two types of creep damage.

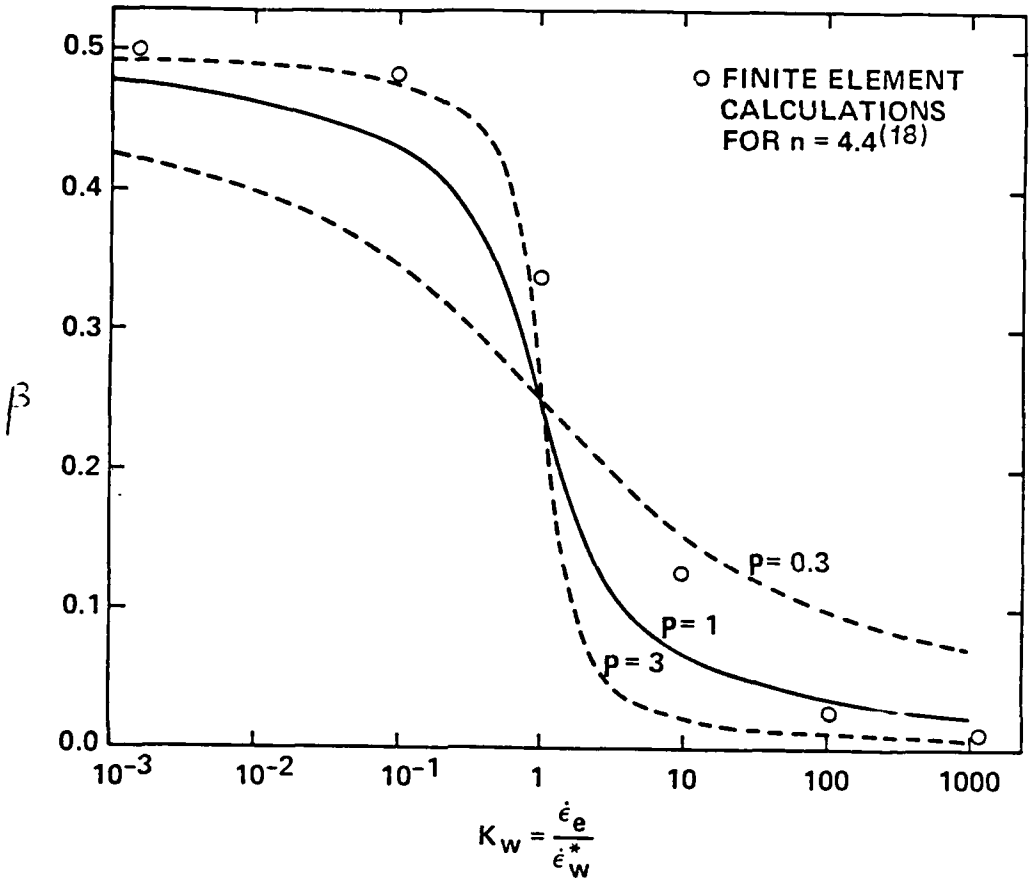

7. Variation of the ratio, β, of strain due to sliding to the applied strain as a function of the applied strain rate $\dot{\epsilon}$ [16].

PERSONNEL

Y.-M. Beissier (M.S. Thesis)	"Influence of Loading Rate on Deofrmation and Fracture Near Crack-Tips at Elevated Temperature"
S. Baik (Ph.D. Thesis)	"Mechanisms of Creep Fatigue Interaction
C. Gandhi	Post-Doctoral Associate
S. Baik	Post-Doctoral Associate (partial)
L.C. Lim	Ph.D. Candidate

PUBLICATIONS

1. "Creep Crack Growth by Cavitation Near Crack Tips," R. Raj and S. Baik, Metal Science Journal, 1980, Aug/Sept. p. 385-394.

2. "An Upper Bound in Strain Rate for Wedge Type Intergranular Fracture in Nickel During Creep", C. Gandhi and R. Raj, Metallurgical Transactions A, 1981, March vol. 12A, pp. 515-520.

3. "Intergranular Creep Fracture in Agressive Environments", R. Raj, Acta Metall. (1982), vol. 30, pp. 1259-1268.

4. "Wedge Type Creep Damage in Low Cycle Fatigue", S. Baik and R. Raj, Metall. Trans. (1282), vol. 13A, pp. 1207-1214.

5. "Mechanisms of Creep Fatigue Interaction", S. Baik and R. Raj, Metall. Trans. (1982), vol. 13A, pp. 1215-1221.

6. "The Effect of Environment on Grain Boundary Internal Friction in an Al-5% Mg Alloy", Acta Metalll. (1982), vol. 30, pp. 499-503.

7. Intergranular Fracture in Bicrystals - II", C. Gandhi and R. Raj, Acta Metall. (1982), vol. 30, pp. 505-511.

8. "Correlations between Cavitation, Creep and Dilation for Multiaxial Loading", Acta Metall. (1983), vol. 31, pp. 29-36.

9. "Creep-Fatigue Interaction in OFHC-Copper", S. Baik and R. Raj, Scripta Metall. (1983), vol. 17, pp. 1087-1090.

10. "On Slip-Induced Intergranular Cavitation During Low-Cycle Fatigue of Nickel at Intermediate Temperature", L.C. Lim and R.Raj, Acta Metall. (1984), in press.

APPENDIX

The following two papers discuss the environmental effects on cavitation and cavitation under multiaxial loading. They are included here because they have not been discussed in the text. Both papers are particularly relevant to nickel base alloys because (a) they are known to be environment sensitive and (b) they exhibit creep crack growth which involves the growth of cavities in a multiaxial stress field ahead of the crack tip.

Acta metall. Vol. 31, pp. 29 to 36, 1983
Printed in Great Britain.

0001-6160/83/010029-08$03.00/0
Pergamon Press Ltd

CORRELATIONS BETWEEN CAVITATION, CREEP AND DILATION FOR MULTIAXIAL LOADING

R. RAJ

Department of Materials Science and Engineering, Cornell University, Bard Hall, Ithaca, NY 14853-0121, U.S.A.

(*Received* 2 *April* 1982; *in revised form* 4 *August* 1982)

Abstract—Intergranular cavitation produces dilation in the specimen. It can also enhance the rate of creep as demonstrated convincingly by experiments of Needham and Greenwood [1] *Metals Sci.* **9**, 258 (1975). Expressions for cavitation enhanced creep, and for cavitation induced dilation are derived. The latter depends only on geometry, but the first is a consequence of the constrained cavity growth mechanism. That mechanism involves redistribution of stress from regions which have cavities to those which do not; as a result the stress on the constraining regions is increased leading to an increase in the measured creep-rate. A comparison of compressive vs tensile tests is suggested as a means of distinguishing the enhancement in creep-rate.

Résumé—La cavitation intergranulaire produit des dilatations dans l'échantillon. Elle peut également augmenter la vitesse de fluage comme l'ont démontré de manière convaincante les expériences de Needham et Greenwood [1] *Metals Sci.* **9**, 258 (1975). Nous avons obtenu des expressions pour le fluage induit par cavitation et pour la dilatation induite par cavitation. Cette dernière ne dépend que de la géométrie, mais la première est une conséquence du mécanisme de croissance forcée des cavités. Ce mécanisme implique une redistribution de la contrainte des régions présentant des cavités vers celles qui n'en ont pas; il en résulte une augmentation de la contrainte dans les régions contraintes provoquant une augmentation de la vitesse de fluage expérimentale. Nous suggérons une comparaison des essais de compression et de traction afin de mettre en évidence l'augmentation de la vitesse de fluage.

Zusammenfassung—Intergranulare Hohlraumbildung führt zu einer Aufweitung der Probe. Sie kann also die Kriechgeschwindigkeit erhöhen, wie die Experimente von Needham und Greenwood [1] *Metals Sci.* **9**, 258 (1975) überzeugend beweisen. Das hohlraumbeschleunigte Kriechen und die hohlraumbedingte Aufweitung werden mathematisch beschrieben. Die Aufweitung hängt nur von der Geometrie ab, das hohlraumbeschleunigte Kriechen jedoch ist eine Folge des eingeschränkten Hohlraumwachstums. Bei diesem Mechanismus werden Spannungen aus Bereichen mit Hohlräumen in Bereiche ohne Hohlräume verlagert; als Folge wird die Spannung auf die einschränkenden Bereiche vergrößert, welches zu einem Anstieg in der gemessenen Kriechgeschwindigkeit führt. Für die Ermittlung des Anstiegs in der Kriechgeschwindigkeit wird vorgeschlagen, Druck- und Zugversuche miteinander zu vergleichen.

INTRODUCTION

Deformation of a cavitating solid can be described by two scalar quantities: an effective strain ϵ_e, which is a measure of the change in shape without a change in volume, and a cavitation strain ϵ_a, which is the fractional increase in volume due to internal cavities. Intuition suggests that in multiaxial loading the mean stress, or pressure, should influence ϵ_a but not ϵ_e, yet Needham and Greenwood [1], and Dyson *et al.* [2] have found that the effective strain-rate does not depend merely on the effective stress, as found in plastic flow of metals, but also on the state of the applied stress. They found that when creep tests were done on copper in a variable hydrostatic pressure, then the rate of creep was influenced by the pressure, even when the effective stress was kept constant. The pressures were too small to influence the self diffusion coefficient. Furthermore, the change in the creep-rate with pressure appeared to be unrelated to the extent of cavitation (as measured by the change in density). Dyson *et al.*, in their work with stainless steel, found a difference in the creep-rate between a tension test and a torsion test, for the same effective stress; but the difference appeared only when cavitation was present. In combination, the two sets of results imply that cavitation is a necessary condition for this effect, although the magnitude of the effect is not related to the extent of cavitation. This means the constitutive equation for cavitation enhanced creep should depend on the stress-state but may not necessarily include a state variable related to cavitation, such as ϵ_a.

Dyson *et al.* proposed that the above phenomenon can be explained in terms of the constrained cavity growth mechanism [3–5]. Their concept is illustrated in Fig. 1. If cavities form preferentially on grain facets aligned nearly perpendicular to the maximum positive principal stress and if the cavities grow by diffusion then grains such as A and B must move apart from each other to accommodate the volume of material which is displaced by cavity growth. They will be constrained from doing so if the creep-rate in the neigh-

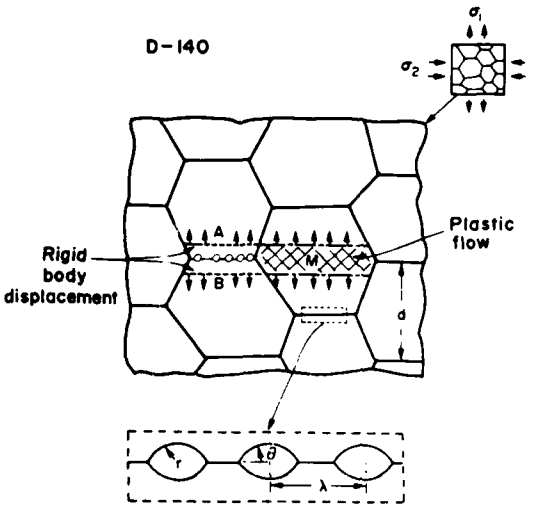

Fig. 1. A schematic illustrating the constrained growth of cavities in a biaxially stressed specimen. The dilation due to cavity growth on transverse boundaries must be accomodated by plastic flow in neighbouring grain matrix.

boring grains is slower than the displacement rate required to accommodate cavity growth. The displacement rate then becomes limited by the rate of creep in adjacent regions, such as M. (It must be remembered that there are different regimes of behavior depending upon the stress, temperature and microstructure. In general, low stress, high temperature, small cavity spacing, and a long time-to-failure favors the constrained growth mechanism [3–5].) This mechanism gives a qualitative explanation of why cavitation, but not the size of the cavities, may influence the creep-rate. In Fig. 1, for example, the load on boundary AB would be transferred to region M leading to an increase in the rate of creep. Yet, the magnitude of the effect will not depend on cavity size. The only condition for load transfer is that if an equal tensile stress were to be applied to region AB and region M, isolated from each other, then AB would elongate at a much faster-rate than M. It has been shown [6, 7] that the displacement rate of AB depends more strongly on cavity spacing than on cavity size.

When cavities form, then one of the conditions for pure plastic flow, that deformation should occur at constant volume, is no longer satisfied. In long term fracture experiments, done under conditions which approach the service conditions, the volumetric strain, in fact, can become the dominant strain [8, 9]. Thus it becomes necessary to distinguish between the shape-change component and the volumetric component of the total strain, before the usual multiaxial stress/strain-rate equations for power-law-creep [2] can be applied.

This paper consists of four parts. First a procedure for separating the creep or the effective strain and the cavitation strain is presented. Next, equations are developed for describing the cavitation-strain in terms of the geometry and the distribution of cavities in the grain boundaries. Third, a power-law constitutive equation, in the presence of growing cavities, is described. Finally, a possible form for the Monkman-Grant equation for use under multiaxial straining is given. The second and the third items are not new in concept. Harris *et al.* [8] have also considered the creep strain arising from the growth of cavities. Although the basic premise of their, and our approach is similar, there are important differences. Their formulation begins from the equations by Hull and Rimmer [10] and Speight and Harris [11] for diffusional cavity growth. It now appears that the constrained cavity growth mechanism is more relevant to long-term creep fracture experiments. In this mechanism, the rate of cavity growth is related to tensile strain, rather than to time as dictated in the Hull and Rimmer approach. Also, in the present work the dependence of the rate growth of cavitation strain on the following parameters: cavity, spacing, grain-size and the di-hedral angle, is explicitly defined.

The third problem, which pertains to the prescription of a constitutive equation for cavitation enhanced effective strain-rate has recently been considered by Dyson *et al.* [2]. The major difference between their results and the equations derived here lies in their assumption that deformation occurs at constant volume; the use of equation (2) in their paper is contingent upon this assumption. While the assumption may be reasonably valid when fracture occurs at large ductilities, it is misleading in long term experiments when the cavitation strain can become a significant fraction of the total strain [9]. The analysis given here distinguishes between creep strain, which is defined for deformation at constant volume, and the cavitation strain.

THE STRAIN-STATE

Any strain state can be described by the three principal strains, ϵ_1, ϵ_2 and ϵ_3, and by the orientation of the axes along which these strains are prescribed. In general then

$$[\epsilon] = \begin{bmatrix} \epsilon_1 & 0 & 0 \\ 0 & \epsilon_2 & 0 \\ 0 & 0 & \epsilon_3 \end{bmatrix} \tag{1}$$

The strain due to change in volume, ϵ_a, and that due to change in shape ϵ_e, can be separated as follows

$$\epsilon_a = \epsilon_1 + \epsilon_2 + \epsilon_3 \tag{2}$$

and

$$\epsilon_e = \frac{2}{3}\sqrt{\frac{1}{2}[(\epsilon_1 - \epsilon_2)^2 + (\epsilon_2 - \epsilon_3)^2 + (\epsilon_3 - \epsilon_1)^2]} \tag{3}$$

The strain ϵ_a is related to the change in density by

$$\epsilon_a = \ln\left(1 - \frac{\Delta\rho}{\rho}\right) \approx -\frac{\Delta\rho}{\rho} \tag{4}$$

where the approximate form holds for small volumetric strain. Here $\Delta\rho/\rho$ is the fractional change in density.

A comparison of equations (2) and (3) shows that ϵ_e and ϵ_a are independent of each other and, therefore, measure different effects of deformation. This also means that if both ϵ_a and ϵ_e are non-zero then at least two principal strains must be measured in order to distinguish between them. As an illustration, consider a uniaxial test. Here we must measure either the transverse strain, ϵ_t, or the change in density, *in addition* to the axial strain, ϵ_z, in order to distinguish between ϵ_a and ϵ_e. Recognizing that two of the principal strains in a uniaxial test are equal, i.e. the transverse strains, we can derive the following expressions

$$\epsilon_e = \tfrac{2}{3}|\epsilon_z - \epsilon_t| = \left|\epsilon_z + \frac{1}{3}\frac{\Delta\rho}{\rho}\right| \tag{5}$$

and

$$\epsilon_a = -\Delta\rho/\rho = \epsilon_z + 2\epsilon_t. \tag{6}$$

If $\Delta\rho/\rho = 0$ then $\epsilon_e = \epsilon_z$, i.e. the axial strain becomes equal to the effective strain.

Measurements of $\Delta\rho/\rho$ in creep experiments show that it usually lies in the range of 10^{-3} to 10^{-2} [1]. Thus in ductile materials the correction from $\Delta\rho/\rho$ in the estimate of ϵ_e in equation (5), is likely to be small. In long term creep-fracture experiments with structural materials, however, the apparent tensile strain at fracture can be small as 1%. In that instance the correction becomes large and it should be implemented.

Since the cavitation strain measures the total volume of all the cavities, it can be estimated theoretically. The task becomes particularly simple if the following assumptions are made: (a) that the shape of the grain boundary cavities is lenticular, and (b) that the number of cavities remains fixed. The first assumption omits the fact that cavities can propagate like cracks under certain conditions [12], and the second that cavities usually increase in number as well as in volume with time [13]. Both factors can be taken into account by increasing the complexity of the calculation.

We assume, as illustrated in Fig. 1, that cavities form only those boundaries which are approximately normal to the applied tensile stress, that their average spacing in a grain facet is λ, and that their shape is described by two parameters r and θ. From this geometry a relationship between ϵ_a and A, the area fraction of cavities in a grain facet can be found, using the expressions in Refs [6, 7]

$$\epsilon_a = \frac{\pi^{3/2} F_v}{8 F_b^{3/2}} A^{3/2} \tag{7}$$

where

$$F_v = \frac{2\pi}{3}(2 - 3\cos\theta + \cos^3\theta), \tag{8}$$

$$F_b = \pi \sin^2\theta, \tag{9}$$

and where $\mathcal{D}$ is the grain size.

In the constrained cavity growth mechanism, the rate of growth of cavities becomes controlled by matrix creep. Thus, even though cavities on a grain facet, such as AB in Fig. 1, grow by diffusion, they do so under a tensile stress which is much smaller than the applied tensile stress. It we assume this local stress to be σ', then the following equation can be written for the rate of growth of damage A

$$\frac{dA}{d\xi} = \frac{(1-A)}{\sqrt{A}} \Big/ \left\{\frac{1}{2}\ln\frac{1}{A} - \frac{3}{4} + A\left(1 - \frac{A}{4}\right)\right\} \tag{10}$$

where ξ is a normalized unit of time, defined as

$$\xi = t \Big/ \left\{\frac{3\sqrt{\pi}}{32}\frac{F_v}{F_b^{3/2}}\frac{kT}{\sigma'\Omega}\frac{\lambda^3}{\delta D_b}\right\} \tag{11}$$

where t is real time, Ω is the atomic volume and δD_b is the boundary width times the grain boundary diffusivity.

Equation (10) is a constitutive equation for describing the rate of accumulation of damage with time. Interestingly, it is universal. The influence of the *microstructural* parameters, such as λ, and the material parameters, e.g. δD_b, and the stress, have been conveniently normalized with respect to time in ξ defined in equation (11). The plot of A vs ξ is given in Fig. 2. If we represent this master curve as function of ξ such that

$$A = g(\xi) \tag{12}$$

and substitute for A in equation (7), we obtain the following equation

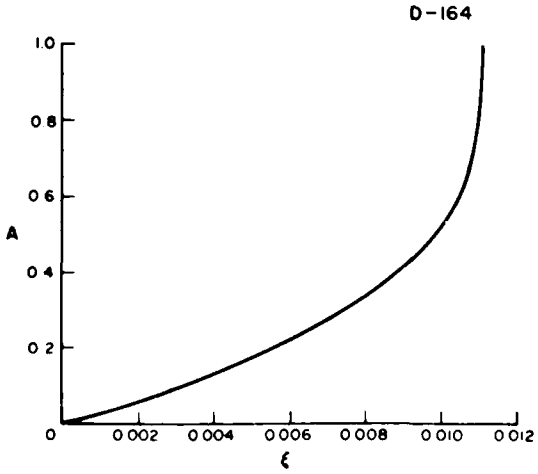

Fig. 2. A plot of A vs ξ obtained from integrating equation (10). Here, A is the cavitation damage and ξ is a normalized unit of time.

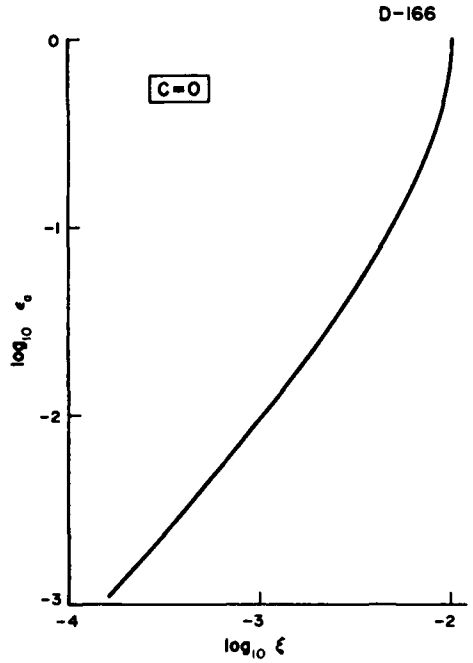

Fig. 3. A master plot showing the change in ϵ_a with ξ. The microstructural parameters, loading parameters, and material parameters have been isolated into parameter C [equation (14)] and into ξ/t [equation (11)].

$$\log_{10}\epsilon_a = C + (3/2)\log_{10}\{g(\xi)\} \tag{13}$$

where

$$C = \log_{10}\left\{\frac{\pi}{12}\frac{2-3\cos\theta+\cos^3\theta}{\sin^3\theta}\right\} + \log_{10}\frac{\lambda}{\mathscr{D}}. \tag{14}$$

Thus equation (13) can be used to compare analysis with the measurement of the change in density, ϵ_a, with time. If plotted on a log-log scale, all data should overlap on a single master curve if the shift factors C and ξ/t are adjusted. Both factors depend on material, microstructural, and loading parameters. C depends on θ, λ, and, as given in equation (14) and ξ/t on θ, λ, σ', and δD_b as described by equation (11). The master curve, which is exactly defined when $C = 0$, is shown in Fig. 3.

The validity of the universal curve in Fig. 3 is nicely demonstrated from the data of Needham and Greenwood [1]. They have obtained plots for $\log \epsilon_a$ vs lot t for various levels of maximum principal stress in tensile tests done with a superimposed hydrostatic pressure. When the data in Ref. [1] are plotted with appropriate shift factors then excellent agreement with the master curve is obtained as shown in Fig. 4.

The analysis by Harris *et al.* [8] differs from the one given here in two respects. First, their analysis is based upon the Hull and Rimmer [10, 11] derivation in which the applied tensile stress acts directly on a transverse grain boundary, whereas in the constrained cavity growth model [3, 4] the local stress on a grain facet may be lower than the applied stress, its magnitude depending on the micromechanics of stress redistribution on the scale of the grain-size. In the present paper this effect is accounted for by using a normalized function of time. The second difference is that a master curve has been derived for the change in relative density with time (Fig. 3). Convincing evidence is presented for the validity of the master curve. Several other experimental studies and a phenomonological formulation of life prediction using ϵ_a as the critical parameter [14] have been reported in the literature. A review of these results is not attempted here.

Before closing this section, one feature of equation (7) is worth emphasizing. It explains how the change in density in the specimen at the time of fracture is related to microstructural parameters θ, λ and $\mathscr{D}$. The relationship between ϵ_a for different values of θ is plotted in Fig. 5. Note that for a given damage, say $A = 0.5$, the change in density increases as θ increases. Also, the change in density is proportional to $\lambda/\mathscr{D}$.

EQUATIONS FOR FLOW

The next step is to consider the constitutive equations for flow in a cavitating solid. In particular we wish to explain how cavity growth can enhance the deviatoric component of the strain-rate, $\dot{\epsilon}_e$. Dyson *et al.* [2] have suggested that the constrained cavity growth mechanism can explain this effect. Although similar in concept, our analysis differs from theirs in that the deformation is separated into two scalar parameters, ϵ_a, which is merely the fractional change in volume and ϵ_e which accounts for the shape change at constant volume. Since the measured principal strain-rates contain a component of volume change, the Levy–Mises constitutive equations of plasticity [15], which apply only when deformation occurs at constant volume, may not be used [2, equation (2)]. The

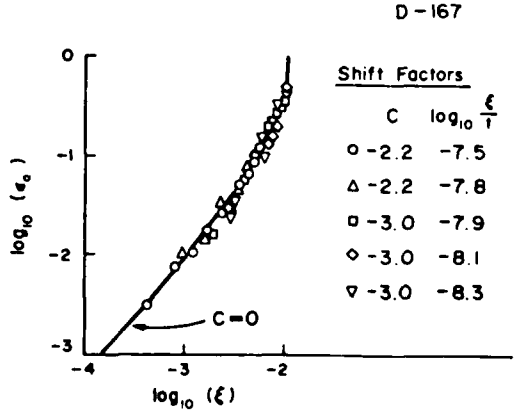

Fig. 4. The master curve in Fig. 5 shows excellent fit with the data obtained by Needham and Greenwood [1].

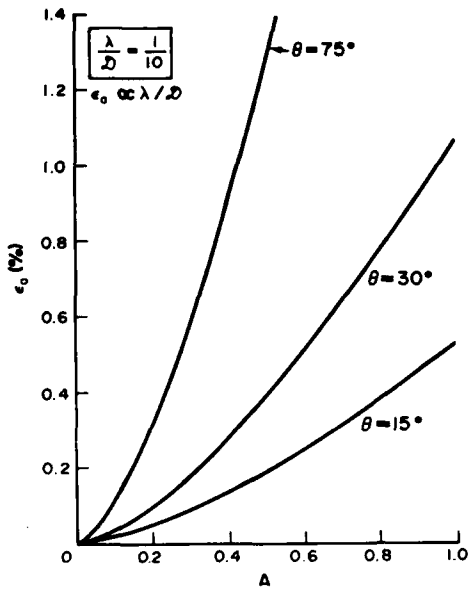

Fig. 5. A plot of ϵ_a vs A, as prescribed by equation (7).

present analysis is restricted to the description of $\dot{\epsilon}_e$ in terms of the principal stresses.

The formulation of creep enhancement is done through a new description of the deviatoric stress. Normal power law creep is represented by the following equation

$$\dot{\epsilon}_e = k_p \sigma_e^n \tag{15}$$

where σ_e, the von-Mises deviatoric stress has the form

$$\sigma_e = \sqrt{\tfrac{1}{2}\{(\sigma_1 - \sigma_2)^2 + (\sigma_2 - \sigma_3)^2 + (\sigma_3 - \sigma_1)^2\}}. \tag{16}$$

In extending equation (15) to the situation of cavitation enhanced creep-rate, some features of the physical mechanism which is responsible for the enhancement must be accounted for. For example in Fig. 1, the strain-rate in direction 1 caused by a compressive principal stress σ_2 remains unchanged because cavity growth in interface AB depends only on σ_1. Also for the same reason a compressive σ_1 will not produce an enhancement in the rate of creep. Creep is enhanced through cavitation only when the principal stress components are tensile. Recognizing the need for distinguishing between a tensile and a compressive principal stress we define a vector δ such that

$$\begin{aligned} \delta_i &= +1 \quad \text{if} \quad \sigma_i > 0 \\ &= -1 \quad \text{if} \quad \sigma_i < 0 \end{aligned} \tag{17}$$

where σ_i are the principal stresses defined by the stress tensor

$$[\sigma] = \begin{bmatrix} \sigma_1 & 0 & 0 \\ 0 & \sigma_2 & 0 \\ 0 & 0 & \sigma_3 \end{bmatrix}.$$

We still define the effective stress by the von-Mises expression but replace σ_1, etc. in that expression by $[1 + \frac{1}{2}\alpha(1 + \delta_1)]\sigma_1$, etc. Thus if $\delta_1 = -1$ then we recover the simple von-Mises form but if $\delta_1 = +1$, then a stress concentration factor of $(1 + \alpha)$ is obtained. Substituting these into the von-Mises equation gives an expression for the deviatoric stress, q_e, which may be used for describing cavitation enhanced creep

$$\begin{aligned} q_e = \sqrt{\tfrac{1}{2}}\,[&\{(1 + \tfrac{1}{2}\alpha)(\sigma_1 - \sigma_2) + \tfrac{1}{2}\alpha(\sigma_1\delta_1 - \sigma_2\delta_2)\}^2 \\ &+ \{(1 + \tfrac{1}{2}\alpha)(\sigma_2 - \sigma_3) + \tfrac{1}{2}\alpha(\sigma_2\delta_2 - \sigma_3\delta_3)\}^2 \\ &+ \{(1 + \tfrac{1}{2}\alpha)(\sigma_3 - \sigma_1) + \tfrac{1}{2}\alpha(\sigma_3\delta_3 - \sigma_1\delta_1)\}^2]^{1/2}. \end{aligned} \tag{18}$$

Note that setting $\alpha = 0$, recovers the pure von-Mises form.

A few specific applications of equations (18) are interesting. First we consider the example of a tensile test superimposed with a hydrostatic pressure, p. Let σ_z be the tensile stress applied to the specimen *inside* the pressure vessel. If $(\sigma_z - p) > 0$, then $\sigma_1 = \sigma_z - p$, $\sigma_2 = \sigma_3 = -p$ and $\delta_1 = 1$ and $\delta_2 = \delta_3 = -1$. If, however, $(\sigma_z - p) > 0$, then $\delta_1 = -1$. Substituting these in equation (18) we obtain

$$q_e = \sigma_z + \alpha(\sigma_z - p) \quad \text{if} \quad \sigma_z - p > 0$$

and

$$q_e = \sigma_z \quad \text{if} \quad \sigma_z - p \le 0. \tag{19}$$

In a torsion test $\sigma_1 = \sigma_s$ and $\sigma_2 = -\sigma_s$ while $\sigma_3 = 0$. Therefore $\delta_1 = +1$, $\delta_2 = -1$ and we obtain that

$$q_e = \sigma_s\sqrt{3}(1 + \tfrac{1}{3}\alpha(\alpha + 2))^{1/2} \approx \sigma_s\sqrt{3}(1 + \tfrac{1}{3}\alpha) \tag{20}$$

where the approximate result neglects second and higher order terms in α. Equations (19) and (20) provide a means of comparing the effective stress in a tensile and a torsion test. If $p = 0$, then the stress concentration factor in a tensile test is $(1 + \alpha)$. In a torsion test is $(1 + 1/3\alpha)$.

The cavitation enhanced effective strain-rate is calculated by substituting q_e instead of σ_e in equation [15].

For the purpose of comparing theory and experiment, the parameter α can be regarded as an adjustable parameter. The equivalent parameter in Dyson *et al.*'s analysis is A_s; and they are related through the equation $(1 + \alpha) = 1/(1 - A_s)$. Upon applying their own analysis to their tension torsion experiments, Dyson *et al.* found that $A_s = 0.33$ gave satisfactory correlation with data. Applying it to the superimposed hydrostatic pressure creep experiments by Needham and Greenwood, a value $A_s = 0.5$ was

needed to give good fit with the data. The application of the present analysis to the same sets of data shows that using $\alpha = 0.42$ (or $A_z = 0.3$) gives good correlation with the tension/torsion data and $\alpha = 1.5$ (or $A_z = 0.6$) gives satisfactory correlation with Needham and Greenwood's data. The difference, although numerically small is a result of the different approach used in calculating the effective strain-rate from the effective stress†.

An extension of equation (18) when the loading is cyclic is given in the Appendix.

MONKMAN–GRANT DUCTILITY

In a simple uniaxal test, when $p = 0$, the minimum creep rate, $\dot{\epsilon}_s$, and time-to-fracture, t_f, are often related by $\dot{\epsilon}_s t_f = \epsilon_{mg}$, a constant in long term fracture tests. The constrained cavity growth model successfully explains this result [3, 4].

If the tensile test is done in a superimposed hydrostatic pressure then the time-to-fracture should correlate with the maximum-principal stress, $\hat{\sigma}_1$ since, in the constrained cavity growth model, the fundamental mechanism of cavity growth is diffusion. The Monkman Grant equation should then take the form

$$k_p \hat{\sigma}_1^n t_f = \epsilon_{mg} \tag{21}$$

In tests with superimposed hydrostatic pressure $\hat{\sigma}_1 = \sigma_z - p$. Needham and Greenwood did in fact find that $(\sigma_z - p)$ and t_f are related through a power-law equation. It would also be interesting to consider if the growth in cavitation strain, ϵ_a, with time also follows a similar rule. A logarithmic plot of ϵ_a normalized with respect to $(\hat{\sigma}_z - p)^{4.7}$, against time is shown in Fig. 6. The results correlate quite well but they separate into two groups, one for $p = 0.1$ MPa and 3.5 MPa, and the other for $p = 6.5$ MPa, 10.4 MPa and 13.8 MPa. A possible explanation is that the cavity spacing for these two groups of results was different. Possibly, the material contained two types of nucleation sites, one requiring a greater threshold stress than the other. Presumably at the high tensile stresses ($p = 0.1$ and 3.5 MPa) both types nucleated leading to a smaller cavity spacing than at the lower stresses ($p \geq 6.5$ MPa) when only one type nucleated.

Whereas the form of equation (21) has a physical basis when tests are done in uniaxal loading under a superimposed hydrostatic pressure, caution must be exercized if it is to be extended to triaxial tensile loading of an isotropic material. The Monkman Grant equation arises from the fact that cavities form inhomogeneously in the material, and, therefore, their growth becomes limited by compatibility constraints. If the material properties were ideally isotropic, i.e.

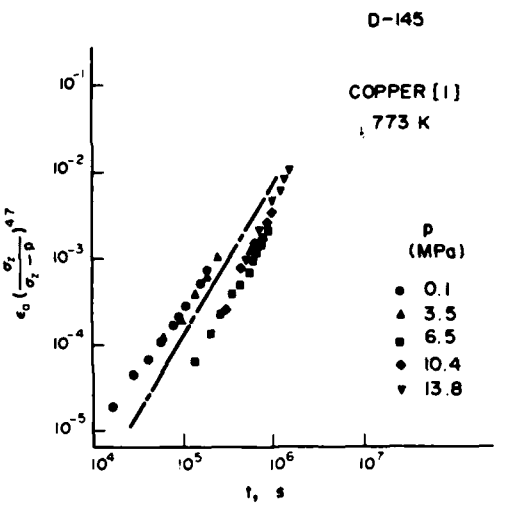

Fig. 6. A normalized plot of data from Ref. [1] showing the correlation between $d\epsilon_a/dt$ and the maximum principal stress.

the grain-size were uniform and equiaxed with all boundaries having the similar density and types of nucleation sites, then under equi-triaxal loading the compatibility constraint should become unimportant, and the simple Hull and Rimmer analysis [7, 10, 11,] should apply. In the author's view [4] any realistic situation is likely to depart considerably from the ideal conditions, and equation (21) should continue to hold even in a general multiaxial stress state.

DISCUSSION

Three inter-related topics have been discussed in this paper. First, the need for separating the cavitation dilation strain and the creep strain is emphasized. Second, it is shown that the growth of cavitation strain with time can be represented on a master curve provided that the strain and the time are normalized with respect to the microstructural and the material parameters such as θ, λ, $\mathcal{D}$ and δD_b. The master curve can be used to predict the residual life of a specimen after it has suffered some cavitation damage, if the normalization parameters C, in equations (13) and (14), and ξ/t, in equation (11), can be calculated. The parameters can be determined experimentally from the knowledge of ϵ_a^f, i.e. the volumetric strain at fracture, and the time-to-fracture, t_f. Substituting $A = 1$ in equation (13) will give $C = \log_{10}\epsilon_a^f$, while the ratio ξ/t may be determined from the knowledge that $\xi_f = 0.011$ (see Fig. 2) and by using $\xi/t = \xi_f/t_f$. Once the shift factors are established the master curve can be used to predict the evolution of damage with time.

The other topic in the paper deals with cavitation enhanced deviatoric creep. The peculiarities of the underlying mechanism for this phenomenon are rather novel in that grain facets which contain growing cavities behave as if they do not support much

† For example, for the case of a torsion test, equation (20) gives the cavitation enhanced effective stress, q_c, which replaces σ_e in equation (15) to give the cavitation enhanced effective strain-rate. Dyson *et al.* get a different result for the effective strain-rate because they calculate it through the Levy Mises equations (their equations 2 and A10).

normal traction, even though the grain boundary has not physically separated. As a result the strain-rate, in a uniaxial test, is enhanced by a factor $(1 + \alpha)^n$ where α is a factor of order one, and where n is the power-law stress exponent. The strain-rate, therefore, may be enhanced by almost a factor of 10. The parameter α has been left as an adjustable parameter in the present analysis. Physically it is a measure of the extent to which the normal stress is transferred from the grain facets on which cavities are growing to the adjacent surrounding regions.

Factors which enhance the strain rate arising solely from the growth of cavities, relative to the rate of creep in the grain matrix, are likely to increase the value of α. Since cavities must grow by diffusion to produce this effect, while the grain matrix is assumed to deform by power-law creep, the following factors are likely to *increase* the value of α: smaller λ because that leads to faster cavity growth by reducing the diffusion distance; smaller applied stress because diffusional cavity growth varies linearly with stress while creep varies as stress to a power of 4 to 5; and intermediate temperatures because diffusional growth is usually dominated by grain boundary diffusion while power-law creep is controlled by lattice diffusion. The enhancement in the creep-rate would also depend upon the spatial redistribution of the load which is shed by the grain facets and transferred to the surrounding grain matrix. In a material with high strain rate sensitivity the load will quickly spread across the load bearing regions and, therefore, lead to a greater increase in the measured creep-rate.

Another interesting point about the above mechanism is that the creep-rate is insensitive to the size of the cavities, the only necessary condition is that cavities should have nucleated and should be growing. This result was confirmed by Needham and Greenwood who found the creep-rate did not depend on the *extent* of prior damage, and by Dyson *et al.* who found that the effect occurred only if the cavities have been pre-nucleated. This raises an interesting application of the phenomenon. Often in engineering materials, there is a need to determine when the cavities nucleate in a stress-rupture test. If an alternate compressive and tensile load were applied to the specimen, then the compressive creep-rate and the tensile creep rate should remain equal until the cavities nucleate. Thereafter, the tensile creep-rate will become significantly faster than the compressive creep-rate.

SUMMARY

1. In long term experiments with structural materials, when the fracture strain is small, the strain due to cavitation (change in volume) and the strain due to creep (shape change only) must be separated. The cavitation strain, ϵ_a, defined in equations (2) and (4) and the creep strain, ϵ_c, in equation (3), are independent quantities in any strain-state.

2. The constitutive flow equation for $\dot{\epsilon}_c$, however, may be coupled to and enhanced by cavitation if the cavities are growing by the constrained cavity growth mechanism. Then the effective stress and $\dot{\epsilon}_c$ are still related through the usual flow equation, but the effective stress, σ_e, is no-longer described by the customary von-Mises equation.

3. A possible new definition for the deviatoric stress, q_e, is given in equation (18). It depends not only on the principal stresses but also on the sign of the principal stresses, since a tensile stress is required to grow cavities by diffusion. The expression contains an adjustable parameter α.

4. α can be determined by comparing the flow behavior in simple tension and simple compression.

5. The relative rates of flow in tension and compression may also be used to evaluate cavity nucleation, since creep enhancement in tension is possible only after the cavities have nucleated.

Acknowledgements—I wish to thank the South West Research Institute, San Antonio, Texas, for allowing me time to study and think about this problem. Support from the Air Force Office of Scientific Research, Grant AFOSR-80-0008, under the direction of Dr A. H. Rosenstein, and by the National Science Foundation through the Materials Science Center at Cornell University, are appreciated.

REFERENCES

1. N. G. Needham and G. W. Greenwood, *Metals Sci.* **9**, 258 (1975).
2. B. F. Dyson, A. K. Verma and Z. C. Szkopiak, *Acta metall.* **21**, 1573 (1981).
3. B. F. Dyson, *Can. Metall. Q.* **18**, 31 (1979).
4. R. Raj and A. K. Ghosh, *Metall. Trans.* **12A**, 1291 (1981).
5. W. Beere, *Acta metall.* **28**, 143 (1980).
6. R. Raj and M. F. Ashby, *Acta metall.* **23**, 653 (1975).
7. R. Raj, H. M. Shih and H. H. Johnson, *Scripta metall.* **11**, 839 (1977).
8. J. E. Harris, M. O. Tucker and G. W. Greenwood, *Metals Sci.* **8**, 311 (1974).
9. M. D. Hanna and G. W. Greenwood, *Acta metall.* **30**, 719 (1982).
10. D. Hull and D. E. Rimmer, *Phil. Mag.* **4**, 673 (1959).
11. M. V. Speight and J. E. Harris, *Metal Sci. J.* **1**, 83 (1967).
12. T.-J. Chuang, K. I. Kagawa, J. R. Rice and L. B. Sills, *Acta metall.* **27**, 265 (1979).
13. B. F. Dyson and D. McLean, *Metals Sci.* **6**, 220 (1972).
14. D. A. Woodford, *Metals Sci.* **3**, 50 (1969).
15. W. A. Backofen, *Deformation Processing*, p. 40. Addison-Wesley, Reading, MA (1972).

APPENDIX

In a fatigue experiment where compressive deformation is imposed after allowing the cavities to grow in tension, some enhancement in the compressive creep-rate may also be expected because the cavities sinter in compression which will lead to a displacement rate of A and B toward each other (see Fig. 1). The enhancement factor in compression is likely to be smaller than in tension. Let the corresponding value of α in compression be α', then the principal stress in the von-Mises equation should be written as $[1 + \frac{1}{2}\alpha(1 + \delta_1) + \frac{1}{2}\alpha'(1 - \delta_1)]\sigma_1$, etc. Note that they

reduce to $[1 + \frac{1}{2}\alpha(1 + \delta_1)]\sigma_1$, and so on, for tension and $[1 + \frac{1}{2}\alpha'(1 - \delta_1)]\sigma_1$ for compression. With these substitutions the expression for von-Mises effective stress becomes:

$$\sigma_e = \sqrt{\tfrac{1}{2}}[\{(1 + \tfrac{1}{2}\alpha + \tfrac{1}{2}\alpha')(\sigma_1 - \sigma_2) + \tfrac{1}{2}(\alpha - \alpha')(\delta_1\sigma_1 - \delta_2\sigma_2)\}^2 + \{(1 + \tfrac{1}{2}\alpha + \tfrac{1}{2}\alpha')(\sigma_2 - \sigma_3) + \tfrac{1}{2}(\alpha - \alpha')(\delta_2\sigma_2 - \delta_3\sigma_3)\}^2 + \{(1 + \tfrac{1}{2}\alpha + \tfrac{1}{2}\alpha')(\sigma_3 - \sigma_1) + \tfrac{1}{2}(\alpha - \alpha')(\delta_3\sigma_3 - \delta_1\sigma_1)\}^2]^{1/2}. \quad \text{(A1)}$$

Acta metall. Vol. 30, pp. 1259 to 1268, 1982
Printed in Great Britain

0001-6160/82/061259-10$03.00/0
Pergamon Press Ltd

INTERGRANULAR CREEP FRACTURE IN AGGRESSIVE ENVIRONMENTS

R. RAJ

Department of Materials Science and Engineering, Bard Hall, Cornell University, Ithaca, NY 14853, U.S.A.

(*Received* 17 *September* 1981; *in revised form* 17 *November* 1981)

Abstract Gaseous species can diffuse along a boundary and oxidize impurities or precipitates. In nickel alloys O_2 can attack C or carbides to produce CO at high virtual pressures. This provides a driving force for cavity nucleation and growth at particle interfaces, which acts in addition to the applied stress in forcing fracture. In this paper it is shown that the oxidation pressure can become comparable to, or even larger than, the stresses normally applied in stress-rupture tests. The dependence of this pressure on temperature and oxygen pressure is derived for various oxidation reactions. Since oxide-dispersion-strengthened alloys are known to be more susceptible to cavitation than precipitate strengthened alloys, it is also possible that internal oxidation enhances cavitation by producing oxide particles from elemental impurities, or by converting metal-carbide and metal-intermetallic interfaces to metal-oxide interfaces. The kinetic steps which may become rate limiting when cavity nucleation and growth is induced by oxidation, are discussed.

Résumé Les gaz peuvent diffuser le long d'un joint de grains et oxyder des impuretés ou des précipités. Dans les alliages de nickel, l' oxygène O_2 peut attaquer le carbone ou les carbures et former de l'oxyde de carbone CO sousde fortes pressions virtuelles. Ceci induit une force motrice pour la germination et la croissance des cavités aux interfaces avec les particules, force mortice qui s'ajoute á la contrainte appliquée pour provoquer la rupture. Dans cet article, nous montrons que la pression d'oxydation peut devenir comparable ou même supérieure aux contraintes appliquées normalement au cours d'essais de rupture sous contrainte. Nous avons obtenu la variation de cette pression en fonction de la température et de la pression d'oxygène pour diverses réactions d'oxydation. Les alliages renforcés par une dispersion d' oxyde présentant plus fréquemment le phénomène de cavitation que les alliages renforcés par des précipités, il est également possible que l'oxydation interne favorise la cavitation en transformant des impuretés sous forme d'éléments en particules d'oxyde, ou en transformant les interfaces métal-carbure et metal-composé intermétallique, en interfaces métal oxyde. Nous discutons les étapes de la cinétique susceptibles de limiter la vitesse lorsque la germination et la croissance des cavités provienent de l'oxydation.

Zusammenfassung—Gasförmige Stoffe können entlang Korngrenze diffundieren und Verunreinigungen oder Ausscheidungen oxidieren. In Nickel-Legierungen kann O_2 bei hohem virtuellem Druck mit C oder Karbiden zu CO reagieren. Dadurch können Hohlräume gebildet werden und an den Ausscheidungsgrenzflächen wachsen. Dieser Vorgang unterstützt die angelegte Spannung bei der Bruchbildung. In dieser Arbeit wird gezeigt, daß der Oxidationsdruck vergleichbar oder sogar größer werden kann ald die Spannung, die üblicherweise in Spannungsbruchversuchen angewendet wird. Die Temperatur- und Sauerstoffdruckabhängigkeit dieses Druckes wird für verschiedene Oxidationsreaktionen abgeleitet. Es ist bekannt, daß Legierungen, die mit Oxidpartikeln gehärtet sind, stärker zur Hohlraumbildung neigen als solche, die mit Ausscheidungen gehärtet sind. Daher ist es auch möglich, daß innere Oxidation die Hohlraumbildung dadurch fördert, daß elementar vorliegende Verunreinigungen zu Oxidteilchen oder Metallkarbiden und Metall-intermetallische Grenzflächen zu Metall-Oxidgrenzflächen umgewandelt werden. Die kinetischen Schritte, die bei Hohlraumnukleation und -wachstum durch Oxidation geschwindigkeitsbestimmend werden können, werden behandelt.

1. INTRODUCTION

Nearly always, engineering materials face aggressive environments during service, which is why a fundamental understanding of phenomena such as hydrogen and liquid metal embrittlement and stress-corrosion cracking is so important. At high temperature, the sensitivity of Ni alloys to air-environment has been reported by Sadananda *et al.* [1, 2, 3]. Recent experiments by Woodford and Bricknell [4, 5, 6] have established beyond doubt that oxygen is an aggressive species in the creep-fracture behavior of nickel base alloys. They have shown [5] that cavities can be induced in Ni even when it contains small amounts of C (~ 100 ppm), and at oxygen pressures which are low enough to be reducing with respect to NiO. They propose that the cavities are bubbles of CO. This reinforces this author's belief that oxygen attack in alloys of Ni does not involve a *new* mechanism of creep fracture, but that it accentuates the usual creep-

fracture mechanism, i.e. cavity nucleation and growth, which occurs even in an inert environment when a tensile stress is applied. This intuition is based on the study of phenomenogical data which compares fracture in 'vacuum' and air environments, e.g. Ref [7]. In general, one observers (a) that although fracture occurs sooner in air than in vacuum, cavitation is still the principal feature of fracture surfaces, and (b) that strong nickel base alloys are often more notch sensitive in air than in vacuum although, again, cavitation is the cause of fracture. The second point can be rationalized as being due to enhanced cavitation by the diffusion of oxygen from the surface.

In this paper, therefore, the earlier work on nucleation and growth of cavities under stress [8, 9, 10], is extended to include the additional thermodynamic driving force for cavitation due to the gas produced by the reaction between O and C (and its compounds). Like the tensile stress across the boundary, the gas pressure attempts to pry the boundary apart. The kinetics of such a process, however, is much more complex, and can be considered only qualitatively. For example, trace impurities can influence the diffusion rate of O through the interface, and surface structure can influence the dissociation reaction of molecular oxygen. One must also think about the mobility of CO molecules in the interfaces, since a boundary which is intact, these must diffuse and coalesce or bind with vacancies to produce a bubble which is larger than a critical size.

The analysis developed here is general and may be applied to other reactions such as sulphides reacting with O_2 to produce SO_2, or with H_2 to produce H_2S, silicides reacting with O_2 to produce SiO, and H_2 with carbides to give CH_4. Since we are concerned here with nickel alloys, primarily, we shall consider only the following reactions

$$Cr_{23}C_6(s) + 3O_2(g) = 23Cr(s) + 6CO(g) \quad (R1)$$

$$2Cr_7C_3(s) + 3O_2(g) = 14Cr(s) + 6CO(g) \quad (R2)$$

$$Cr_3C_2(s) + O_2(g) = 3Cr(s) + 2CO(g) \quad (R3)$$

$$2CO(g) + O_2(g) = 2CO_2(g) \quad (R4)$$

where the letters in brackets stand for solid (s) and gas (g). The products in reactions (R1), (R2) and (R3) can react further with O_2. Carbon-monoxide can oxidize into CO_2, as given by reaction (R4). In fact, at temperatures of interest and at $p_{O_2} = 1$ (where p is the equilibrium partial pressure), oxidation to CO_2 is a favored reaction, i.e. p_{CO_2} will be greater than p_{CO}, although, kinetically, it may be more difficult to obtain CO_2 because the reactions must occur in the solid state. Similarly, Cr may oxidize into Cr_2O_3 which will also increase the CO pressure. In nickel base superalloys, the presence of excess Cr would suggest that reactions (R1) to (R3) rather than those producing Cr_2O_3, are applicable. Finally, for those instances when free C is present we consider the reaction:

$$2C + O_2 = 2CO. \quad (R5)$$

In the following sections, thermodynamics and kinetics are considered separately. The discussion concentrates more on nucleation rather than on growth because it is felt that the production rate of CO or CO_2, which may be limited by the diffusional transport of O from the surface, may not be fast enough to keep up with the growth of cavities when they grow large, but may have significant influence when cavities are of nm dimensions. The treatment, however, fully includes the issues related to both nucleation and growth.

2. THERMODYNAMICS

2.1 *Gas pressure as a driving force for nucleation and growth*

Consider a cavity in a grain boundary. A normal traction, σ_x, is applied across the boundary and the cavity is pressurized with a gas at pressure, p. Assume now that the cavity grows by a volume δV, by the transport of matter from the cavity surface to, and into, the grain boundary. In such case the elastic energy may be neglected [8] and the change in energy of the system, δW, will involve the work done by σ_x, by p, and by the 'sintering pressure', $2\gamma/r$ where γ is the surface energy and r is the radius of curvature (assuming that both radii of curvature in the surface are equal). Thus

$$\delta W = \int_S \delta\chi \left(p - \frac{2\gamma}{r}\right) dS + \sigma_x \, \delta V \quad (6)$$

where $\delta\chi$ is the small normal surface displacement, and the integral represents integration over the surface S. If $p \gg (2\gamma/r)$ *or* if the cavity is of an equilibrium shape so that r is uniform at all parts of the cavity surface then $(p\text{-}2\gamma/r)$ becomes constant and (3) reduces to

$$\delta W = \left(p - \frac{2\gamma}{r} + \sigma_x\right) \delta V. \quad (7)$$

It follows that in calculations of cavity nucleation and growth σ_x may be replaced by $(\sigma_x + p - 2\gamma/r)$ provided that the cavity has a near equilibrium shape *or* if $(\sigma_x + p) \gg 2\gamma/r$. Earlier, this author has proposed a diffusive model for cavity nucleation [10] where a cavity grows by clustering of vacancies until the cavity becomes super-critical. For sub-critical voids, the surface-energy factor is dominant and the cavity grows slowly; in this instance equation (7) should apply because the cavity is small and slow growing so that it would retain its equilibrium shape. When the cavity is much larger than the critical size then the $2\gamma/r$ term should become relatively small and again equation (7) should apply, provided that $\delta\chi$ is independent of S. Caution is needed when the cavity is just a bit bigger than its critical size.

In equation (7), p is the mechanical pressure of the gas. If the gas is produced by chemical reactions (R1 thru R5), then the virtual pressure, also p, will be given by:

$$f = \Gamma p \tag{8}$$

where f is the activity, or the fugacity, and Γ is the activity coefficient. f, thus, is determined through the free-energy of the reaction in question, and becomes the 'chemical' driving force for cavity nucleation. We now discuss the magnitudes for f and p.

2.2 f_{CO} *Produced by reactions between C, carbides and* O_2

The fugacity of CO for reactions (R1 to R5) is calculated in this section. The standard free energy of formation of the different carbides of Cr, CO and CO_2, and Cr_2O_3, are listed in Table 1. The values for the carbides have been taken from Ref. [12] because they were obtained by seeking equilibrium with CO gas and because they are in agreement with other measurements where equilibrium with CO was also used to obtain thermodynamic data [14]. These numbers differ slightly from those given in Ref. [13] (by less than 3% for $Cr_{23}C_6$, 4% for Cr_7C_3 and 8% Cr_3C_2). For a recent review see Ref. [15].

The fugacity of CO is plotted as a function of temperature and p_{O_2} for reactions of O_2 with $Cr_{23}C_6$, Cr_7C_3, Cr_3C_2 and C, in Fig. 1. Note that $Cr_{23}C_6$ gives the smallest values for the fugacity and C the highest. Typically, at 1000 K, the values for $Cr_{23}C_6$ are about 10^7 at $p_{O_2} = 1$, and 10^3 at $p_{O_2} = 10^{-8}$. For pure C the fugacities are a factor of 3×10^3 higher, at 1000 K.

At this point it would be interesting to estimate the virtual CO pressure in experiments of Bricknell and Woodford [5]. Their technique for controlling p_{C} was to pack the Ni-specimens which contained some C in Ni:NiO powder at 1273 K, which fixed the O_2 activity at $p_{O_2} = 3 \times 10^{-11}$, and then see if bubbles were produced in the boundaries and they were. *Assuming* a carbon activity of one, we obtain from Fig. 1, that $f_{CO} = 7 \times 10^3$. If *instead* we assume that a_c, the carbon activity, was equal to the average C concentration (100 ppm by weight), then $a_C = 5 \times 10^{-4}$, which reduces f_{CO} to 3.4. At these low pressures once may assume the $\Gamma = 1$, which would mean an effective CO pressure, $p_{CO} = 0.34$ MPa (using equation 8). Since cavities were observed under these conditions, one may infer that $a_c > 5 \times 10^{-4}$ because of non-equilibrium segregation in the boundaries. There is also the possibility that CO_2 instead of CO was being produced. That reaction at 1273 K and $p_{O_2} = 3 \times 10^{-4}$, yields $p_{CO_2} = 21$ MPa, which is a stress large enough to cause cavitation in pure nickel. The enhancement factor, when CO_2 rather than CO is the reaction product, is given in Fig. 2, and was obtained by considering reaction (R4).

The assumptions made in the calculation of curves in Figs 1 and 2 need to be re-emphasized. The activities of Cr, C and the carbides have been assumed to be unity. While this is probably true for the carbides, since they do not dissolve significant amount of impurities, the activities of Cr and C would depend on the alloy composition and on whether or not the boundary segregation of these impurities is in equilibrium with the matrix. Decreasing C activity decreases f_{CO}, while decreasing Cr activity increases f_{CO}. In case of $Cr_{23}C_6$, f_{CO} approximately increases as $1/a_{Cr}$ [4]. Possibly a more accurate estimate of activities in real alloys can be done, but, in the author's view a systematic experimental study on the ternary Ni-Cr-C system is first necessary before attempting to apply the analysis to more complex alloys. Another assumption, that Cr rather than Cr_2O_3 is the reaction product, is justified on the basis that excess Cr is usually present in the nickel-base alloys. However, for sake of completeness, analytical expressions for f_{CO} for this and the other reactions, are given in Table 2.

The fugacity of gases, f, can be related to their partial pressure, p, through the expression in equation (8). For low values of f, up to a few atmospheres, the behavior should remain ideal, and the activity coefficient $\Gamma = 1$. In the following section we describe a method for obtaining approximate values of Γ at *large* partial pressures of the gas.

3. FUGACITY OF NON-POLAR GASES AT HIGH TEMPERATURE AND PRESSURE

3.1. *Equation of state*

At high pressures the compressibility, and, therefore, the free energy of gases becomes pressure depen-

Table 1. Free energy of formation

Compound	Standard free energy of formation ΔG_0	ΔG_0 (J mole^{-1})	Reference	Temperature range K
CO (g)	-111.6×10^3	$-87.57T$	11	298–2500
CO_2 (g)	-393.8×10^3	$-0.84T$	11	298–2000
$Cr_{23}C_6$(s)	-321.9×10^3	$-76.5T$	12	1150–1300
Cr_7C_3 (s)	-147.1×10^3	$-36.37T$	12	1100–1720
Cr_3C_2 (s)	-68.6×10^3	$-18.4T$	12	1300–1500
Cr_2O_3 (s)	-1121.8×10^3	$+252.8T$	13	800–1600

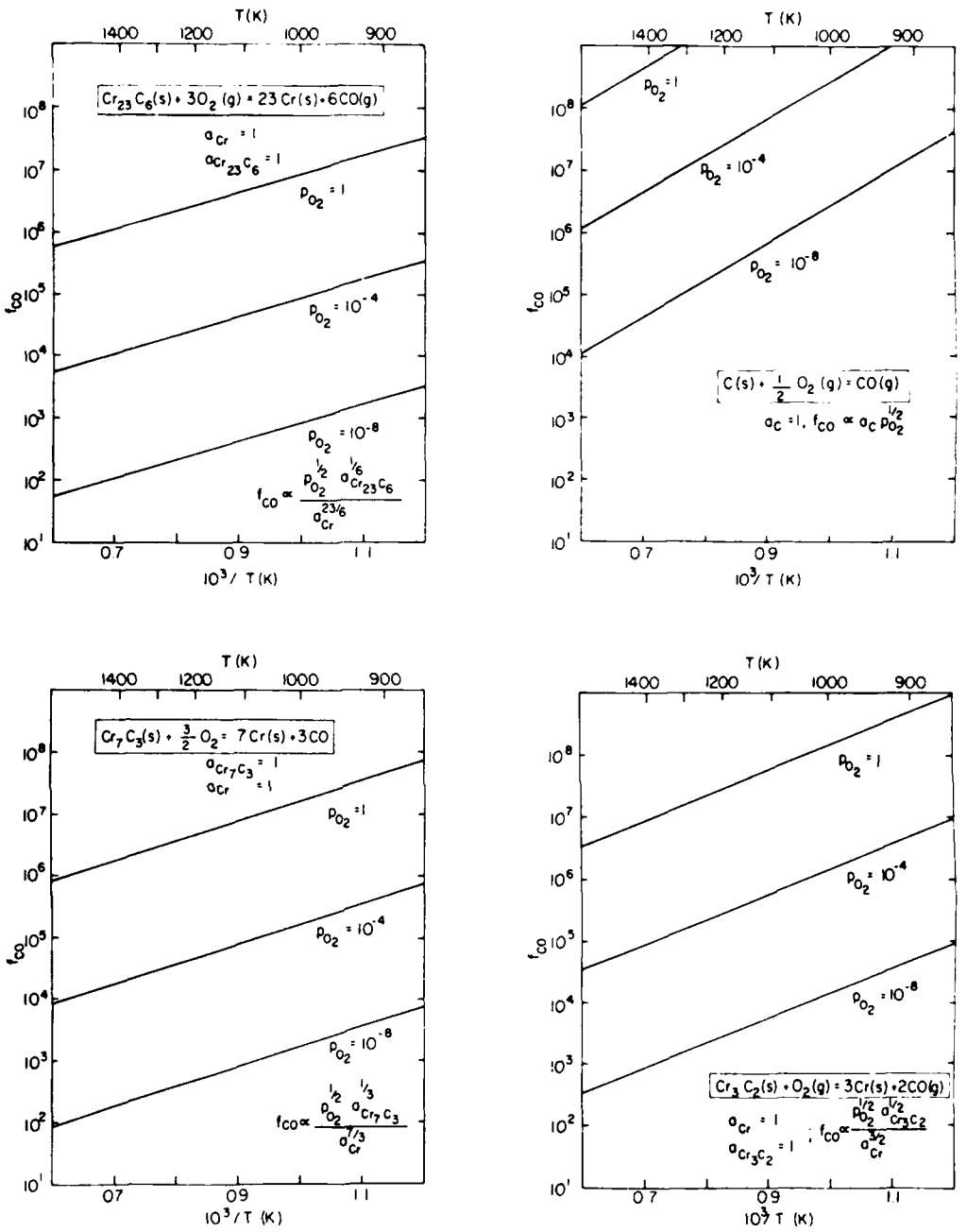

Fig. 1. CO fugacities as a function of temperature and oxygen pressure for different oxidation reactions.

dent. If gases are non-polar†, the interaction between the molecules may be described by van-der Waal's equation. This concept was used by Maron and Turnbull [17] to express the equation of state of a non-polar gas as:

$$pV = RT + \sum_{n=1}^{4} \alpha_n p \qquad (9)$$

where $\alpha_n(T)$ are the virial coefficients. It was shown that (9) was obeyed by several gases (H_2, CH_4, He, CO_2, HNO_3, C_2H_4, O_2, CO, C_3H_8, C_2H_6) in the range 203 to 873 K, and 1 to 1000 bars.

Equation (9) can be substituted in equations $(\partial G/\partial p)_T = V$ and $\delta G = RT\delta(\ln f)$, and equation (8) to

† For ideal non-polarity, the bonds in the molecule should be 100% covalent, and 0% ionic. A comparative measure of the extent of ionicity in different gases can be obtained by applying Paulings' approximation(16). This gives that the C–O bond is 19% ionic and the C–H bond is 8% ionic. We will show that the van-der Waal's approximation gives reasonable results for CH_4 at pressures up to 10^4 atm. We, therefore, feel comfortable in applying the same analysis to CO and CO_2.

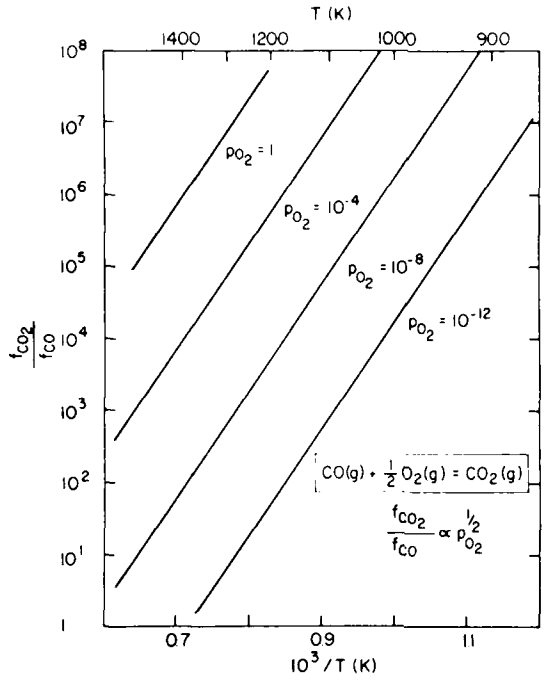

Fig. 2. Relative fugacity of CO_2 and CO for oxidation of CO.

give:

$$\ln I = \sum_{n=1}^{4} \frac{\alpha_n p^n}{nRT} \tag{10}$$

Maron and Turnbull argue that equation (10) should be universal if p and T are normalized with respect to the critical values, p_c and T_c, in van-der Waal's equation such that

$$p_r = \frac{p}{p_c} \quad \text{and} \quad T_r = \frac{T}{T_c} \tag{11}$$

where p_r and T_r are the reduced or normalized quantities. With these substitutions (10) becomes

$$\ln I = \sum_{n=1}^{4} a_n \frac{p_r^n}{nRT_r} \tag{12}$$

where

$$a_n = \alpha_n(T_r) \frac{p_c^n}{T_c} \tag{13}$$

Maron and Turnbull have shown that the above parametric description fits the P,V,T data to an accuracy of better than 5%. The coefficients a_n are listed in Table 3.

Table 2. Equilibrium values of CO fugacity for different oxidation reactions

$CO(g) + \frac{1}{2}O_2(g) = CO_2(g)$	$\frac{f_{CO_2}}{f_{CO}} = p_{O_2}^{1/2} \times 2.9 \times 10^{-5} \exp(282.2\ \text{kJ mole}^{-1}/RT)$
$Cr_{23}C_6(s) + 3O_2(g) = 23Cr(s) + 6CO(g)$	$f_{CO} = 8.2 \times 10^3 \frac{p_{O_2}^{1/2} a_{Cr_{23}C_6}^{1/6}}{a_{Cr}^{23/6}} \exp(58\ \text{kJ mole}^{-1}/RT)$
$2Cr_7C_3(s) + 3O_2(g) = 14Cr(s) + 6CO(g)$	$f_{CO} = 8.9 \times 10^3 \frac{p_{O_2}^{1/2} a_{Cr_7C_3}^{1/3}}{a_{Cr}^{7/3}} \exp(62.6\ \text{kJ mole}^{-1}/RT)$
$Cr_3C_2(s) + O_2(g) = 3Cr(s) + 2CO(g)$	$f_{CO} = 1.3 \times 10^4 \frac{p_{O_2}^{1/2} a_{Cr_3C_2}^{1/2}}{a_{Cr}^{3/2}} \exp(77.3\ \text{kJ mole}^{-1}/RT)$
$C(s) + \frac{1}{2}O_2(g) = CO(g)$	$f_{CO} = 3.8 \times 10^4\, p_{O_2}^{1/2} a_c \exp(111.6\ \text{kJ mole}^{-1}/RT)$
$4Cr_{23}C_6 + 81O_2 = 46Cr_2O_3 + 24CO$	$f_{CO} = 3.9 \times 10^{-22} \frac{p_{O_2}^{81/24} a_{Cr_{23}C_6}^{1/6}}{a_{Cr_2O_3}^{23/12}} \exp(2208\ \text{kJ mole}^{-1}/RT)$

Table 3. Numerical expressions for the coefficients a_n in equation (13). These numbers are *not* dimensionless, they have been calculated such that $R = 0.082054$ liter bar K^{-1} $mole^{-1}$ and p and V are expressed in bars and liters in equations (9)–(13)

$$a = A_0 + \sum_{m=1}^{6} A_m T_r^m$$

	A_0	A_1	A_2	A_3	A_4	A_5	A_6
a_1	1.0196×10^{-2}	-2.1420×10^{-2}	0	-3.2548×10^{-2}	0	0	0
a_2	0	0	3.6991×10^{-3}	0	-4.3022×10^{-3}	0	$1.8.39 \times 10^{-3}$
a_3	0	0	-1.251×10^{-4}	0	4.6408×10^{-4}	0	-1.5573×10^{-4}
a_4	0	0	1.7019×10^{-6}	0	-1.1221×10^{-5}	0	3.2830×10^{-5}

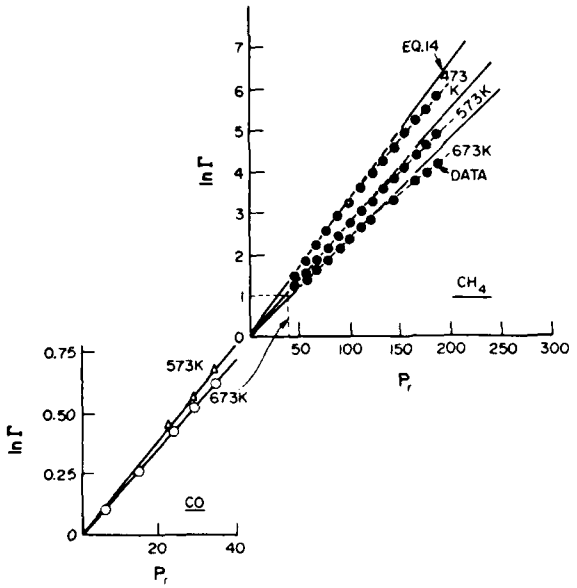

Fig. 3. Variation of Γ, the activity coefficient, with p for CH_4 and CO. The CO data is from Refs [19 and 20] and the CH_4 data from Ref. [18].

3.2 *Applications of equation (12) to carbon-monoxide gas*

Compressibility data for CO extends up to 1200 bars and 673 K. Since the fugacities calculated for carbide oxidation reactions (Fig. 1) can be up to $\times 10^3$ higher, we must consider the suitability of extrapolating equation (12) to higher pressures. Since that polynomial contains terms with T_r and p_r raised to a high power, small errors in the numerical coefficients will lead to large discrepancies in the estimate of Γ. To reduce this uncertainty we consider only the first order term in equation (12). Thus

$$\ln \Gamma = A_r \frac{p_r}{T_r} \tag{14}$$

where A_r is a universal dimensionless constant which must be determined from data. Keeping in mind that the critical parameters for CO and CH_4 are

$$\begin{aligned} &\text{CO: } p_c = 35.0 \text{ bars} \qquad T_c = 134.18 \text{ K} \\ &CH_4\text{: } p_c = 45.8 \text{ bars} \qquad T_c = 190.68 \text{ K} \end{aligned} \tag{15}$$

we obtain the plots shown in Fig. 3 for the fugacity data, according to equation (14). The fit with (14) is quite good when $p_r < 75$, but above that the value of Γ given by (14) overestimates the data. By extrapolation, we may assume that the value of Γ, if calculated from equation (14), will always be $\geq$ to the actual value. If this value is substituted in equation (8), then we shall obtain the lowest possible value for p.

The universality of equation (14) is checked by calculating A_r for CO and CH_4 at different temperatures. These results, on the basis of the straight lines drawn in Fig. 3, are tabulated in Table 4. A mean value of $A_r = 8.57 \times 10^{-2}$ is obtained with a maximum deviation of less than 7%.

The equilibrium values for p_{CO} are obtained by applying equations (14) and (8) to the fugacity curves in Fig. 1. The results for the reactions (R1) and (R5) are shown in Fig. 4. Remember that these are subject to the assumptions discussed in this section. In general we expect that the numbers are quite good as long as p_{CO} is less than 3×10^3 bars. When the estimated p_{CO} is greater, then the real values are likely to be even higher than those derived in Fig. 4. Nevertheless results in Fig. 4 provide some interesting insights. When $p_{O_2} = 1$, the CO pressure will be greater than 10^3 MPa, a value which is even larger than the stress applied in most stress-rupture tests. The pressure falls sharply when the p_{O_2} drops below 10^{-8} bars. As a guideline, one can expect that when p_{O_2} is below 10^{-10} bars, the oxidation reaction would be thermodynamics limited, while above 10^{-8} bars the kinetics of the reaction may be more important. Also, for a fixed value of p_{O_2} the environmental attack should be most severe at intermediate temperatures; at high temperatures p_{CO} becomes small, while at the lower temperatures the kinetics becomes slow. The question of kinetics is discussed in the next section.

4. KINETICS

4.1 *The heterogeneous nucleation model*

The mechanism of cavity nucleation in creep-fracture remains controversial. Limited observations suggest that cavities do not nucleate below a threshold stress [21], that they increase in number with time [22] and that triple junctions formed by second phase particles and grain boundaries are the preferred sites for nucleation. There is more in the literature

Table 4. A tabulation of the constant A_r in equation (14) based upon thermodynamic data for CO and CH_4

	T K	p (range) bars	T_r	p_r (range)	A_r
CO	673	25–1200	5.02	0.7–34.3	9.18×10^{-2}
CO	573	25–1200	4.27	0.7–34.3	8.46×10^{-2}
CH_4	673	2000–8500	3.53	43.7–185.6	8.54×10^{-2}
CH_4	573	2000–8500	3.01	43.7–185.6	8.34×10^{-2}
CH_4	473	2000–8500	2.48	43.7–185.6	8.35×10^{-2}
				Average value	8.57×10^{-2}

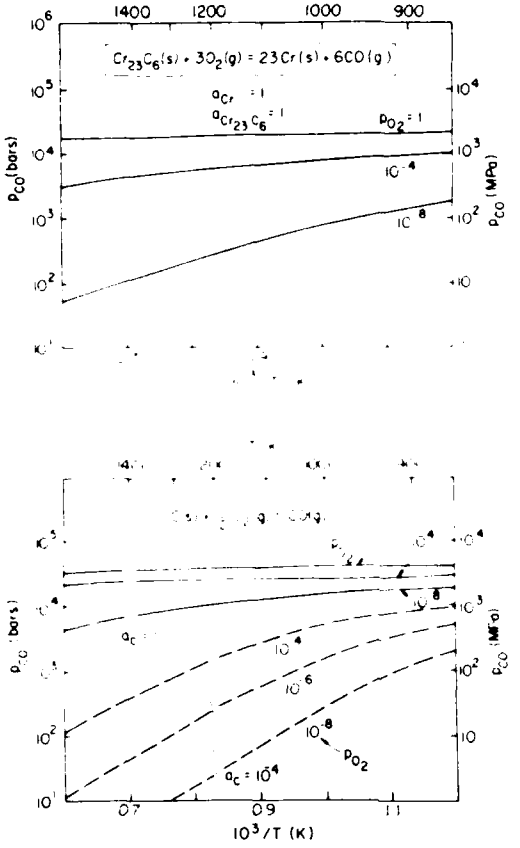

Fig. 4 Carbon-monoxide partial pressure for two oxidation reactions. a_c is carbon activity.

than cited here, but still further work is needed before the picture becomes clear. For the present, we shall assume that the model published earlier [10] is viable. The cavities can nucleate under applied stress by a mass transport process provided that the barrier for cavity nucleation due to surface energy, is not very large. A useful physical parameter to characterize the nucleation process is an incubation time which marks the transition fr[om] extremely slow, sub-critical growth of cavities to fast, super-critical growth. We can appreciate that the incubation time will depend upon the volume of the cavity of critical size (expressed in units of atomic volume) and upon the diffusion rate of vacancies. The critical volume, r_c, can be shown to depend on two factors: the driving force for nucleation, which is $(\sigma_1 + p)$, and the site of nucleation in the following way

$$r_c = \left(\frac{2\gamma}{\sigma_1 + p}\right)^3 F_1 \Omega_m$$

where γ is the surface energy, Ω_m is the weighted molecular† volume and F_1 is a factor which depends on the site of nucleation. Note that r_c is dimensionless. It has been shown that the smallest values of F_1 should be achieved at junctions of particles and grain boundaries [10], as shown in Fig. 5. F_1 would depend on the dihedral angles α, α', β and β' all of which must satisfy equilibrium, while at the same time, the radius of curvature r is uniform at all surfaces of the boundary. The particle shape and the surface energies will influence F_1 which in certain instances may even become zero (for example in a matrix matrix matrix triple grain junction F_1 becomes zero if $\alpha < \pi/6$). Also, F_1 may well vary from one particle to another giving rise to a distribution in the values for nucleation time. Experience suggests that incubation time would be within the realm of measurement at temperatures near $0.5\ T_m$ when r_c is of the order of 10^3–10^4 atomic volumes [10].

The oxidation reaction can hasten the incubation time because the critical nucleus size will become smaller (equation (6)) and because the large CO molecules may accelerate cluster growth by trapping vacancies.

4.2 *Diffusion reactions*

Nucleation and growth of cavities by p_{CO} involves several sequential reactions. For example, as shown in the schematic in Fig. 6, dissociation of oxygen to atomic O at the surface, diffusion of O along the boundary to the carbide precipitates, production of CO by oxidation and clustering of CO with each other and with other vacancies to form cavities, and diffusion of CO back out to the surface. In principle any one of the above reactions can become rate limiting. Different scenarios and conditions are summized in Table 5. The comments are left qualitative because at this point, rigorous analysis including diffusion, interface reaction kinetics and cluster formation would not lead to further insights. Instead we wish to emphasize the need for more definitive and simple experiments.

Some general statements can be made on the basis of the listing in Table 5. High O solubility coupled with low CO solubility in the interface will promote nucleation and vice-versa. A small carbide spacing (this should be about equal to the distance of the

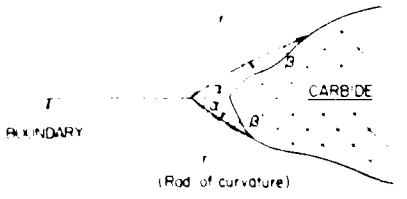

Fig. 5 The parameter F_1 depends on the site of nucleation. It is the smallest (implying easier nucleation) at the triple junction between a grain boundary and a second phase particle. It depends on the equilibrium dihedral angles α, α', β and β' when all cavity surfaces have uniform radius of curvature (r). Particle shape and interface energies, therefore, will influence F_1.

† Since the cavity may contain vacancies, CO and CO_2 molecules, Ω_m is the average volume per molecule for a given composition of the 'gas'.

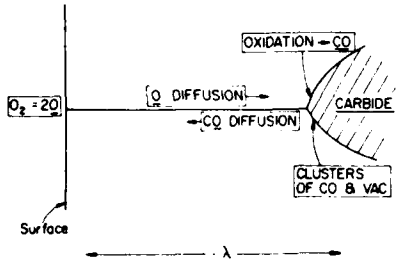

Fig. 6. Illustration of various kinetic processes which can limit cavity nucleation.

carbides from the surface) will also promote nucleation, while presence of trace impurities which inhibit O diffusion will suppresss nucleation. Because *CO* molecules are large they would induce considerable strain energy which should relieve by having vacancies or other CO molecules next to it. This would give rise to a large binding energy and help nucleation. The O=O bond is quite strong, 4.7 eV and there may be instances where dissociation of $O_2 \rightarrow 2O$ may become important.

The solubility of O and CO are likely to be strongly influenced by the hydrostatic component of the applied stress (because the partial molar volume of solution may be large), which means that the stress-state can affect environmental attack. In general a tensile mean stress, as found at notch roots, will promote nucleation.

Theoretically, the highest gas pressures which can be achieved will be those calculated from thermodynamics in the previous section. In practice they may be lower because of the kinetic reasons described above. Another limit on the maximum pressure is the yield strength of the material; if it becomes greater than a critical value then the void will begin to grow plastically. An approximate value for this critical pressure can be obtained by drawing an analogy with a thick walled sphere which yields up to a diameter c when the cavity of diameter, a, is pressurized to pressure, p_{max}. If the material is non-hardening with a flow stress Y, then it may be shown that [23]

$$p_{max} = \tfrac{2}{3} Y \left[1 + \ln\left(\frac{c}{a}\right)^3 \right] \qquad (17)$$

The 'burst' pressure can be estimated by setting c/a equal to (particle spacing)/(particle size). Assuming the latter to be about 5, we get that $p_c \approx 4Y$.

A good discussion of the kinetics of void growth in the H_2 attack (CH_4) problem in steels can be found in Ref. [24].

5. SUMMARY

Oxidation of carbides (or carbon) by oxygen transported from the surface via grain boundaries can produce CO at high pressures. This pressure adds to tensile applied stress in promoting nucleation and growth of cavities. Reasonable thermodynamic calculations have been done, which show that the gas pressure can be as large as 1000 MPa when $Cr_{23}C_6$ is oxidized at 1000 K and $p_{O_2} = 1$. At $p_{O_2} = 10^{-8}$ the pressure reduces to about 100 MPa and at $p_{O_2} = 10^{-12}$ to about 1 MPa. From thermodynamic considerations it would appear that environmental effect would begin at about $p_{O_2} > 10^{-10}$ bars. The only data of this type in the literature, by Shahinian *et al.* [2, 3], is in agreement with this. They found that low cycle fatigue life of Ni at 823 K [2] changes sigmoidally with increasing p_{O_2}. The fatigue life first begins to drop when $p_{O_2} > 10^{-9}$ and then saturates when $p_{O_2} > 10^{-4}$. This would also be expected from the thermodynamic calculations: p_{CO} would be much smaller than the applied stress when p_{O_2} is low, while p_{CO} becomes large but insensitive to p_{O_2} when $p_{O_2} > 10^{-4}$ (see Fig. 4), because fugacity begins to rise non-linearly with pressure. The need for further careful and systematic experimental work is obvious.

Whereas the thermodynamic criterion may provide a qualitative explanation for environmental attack in

Table 5. Kinetic limitations to cavity nucleation

Condition		Possible causes
Slow O diffusion	i.	Trace impurities and traps in the boundary suppressing *O* diffusion
	ii.	Low *O* solubility
	iii.	Large λ (see Fig. 6)
Slow (interface limited) Oxidation reaction		*Before nucleation of a cavity*
	i.	Coherent or semi-coherent carbide matrix interface
	ii.	Low mobility of *CO* in the interface
		After nucleation of a cavity
	i.	Structure of the carbide free surface
Fast cluster growth for cavity nucleation	i.	High binding energy between *CO* molecules with each other and with vacancies
	ii.	Low *CO* solubility in the interface
Slow CO diffusion	i.	Low *CO* solubility
	ii.	Trace impurities and traps in the boundary which suppress *CO* diffusion
	iii.	Large λ (see Fig. 6)

Ni, the oxygen attack in nickel-base structural alloys appears to be very sensitive to alloy composition, suggesting the importance of kinetics. At this point it is not even possible to estimate whether nor not Q diffusion is the boundary is a rate limiting step for lack of grain boundary diffusion data for Q in Ni. There is circumstantial evidence that this may be important because addition of trace B appears to hinder Q diffusion, thereby delaying cavitation [6].

7. ADDITIONAL REMARKS

Structural nickel base alloys contain a considerable amount of Cr and Al, partly to enhance creep resistance, but also to provide a protective oxide on the surface against corrosion. A tenacious oxide layer would reduce the oxygen activity at the oxide-metal interface to a near equilibrium level, for example, about 10^{-30} to 10^{-21} at 1000 to 1300 K assuming a Cr Cr_2O_3 interface. Such low p_{O_2} would preclude the cavitation mechanism discussed so far. Why then are structural alloys environment sensitive? The question can be answered in several ways.

Perhaps the most important reason is that deformation can break the surface layer permitting subsurface diffusion of Q. Grain boundary sliding can produce offsets at the surface. Propagation of creep cracks, or crack-tip sharpening in fatigue loading, can continually expose fresh metal surface. Circumstantial support for this idea comes from the experience [26] that often notch sensitivity and environment sensitivity of alloys goes hand in hand. Also alloys which show stress-rupture strengthening in oxygen with smooth tensile specimens, may exhibit oxygen attack if notched specimens are used. Presumably localized slip at notch root breaks the oxide scale. Experience also suggests [26] that nickel-base alloys which have excellent resistance to simple corrosion, can be quite susceptible to stress corrosion cracking at elevated temperature.

In addition to the internal gas production, internal oxidation of impurities or carbides, which produces new oxide precipitates or an oxide shell on existing precipitates can also promote cavity nucleation. The reason is that, nearly always, oxide dispersion alloys have poor resistance to cavitation. Apparently, at least in alloys of Cu and Ni, oxide precipitates are poorly adhered to the metal. Internal oxidation of impurities in the boundaries could occur at fairly low activities of oxygen, although, again, if a very stable oxide such as Al_2O_3 or Cr_2O_3 forms on the surface then some mechanism must be available for penetrating the oxide layer.

There are two other interesting observations in this context. Oxide dispersion strengthened Ni alloys (Ni-Cr-ThO_2), with equiaxed grain structure are known to be much less environment or notch sensitive than the precipitation strengthened alloys; presumably these are already prone to cavitation because they contain oxide particles so that oxygen attack can do no further harm. The second observation is that whenever environmental attack is severe, the addition of trace B and Zr has a dramatic beneficial effect. In Ni C alloys this effect has been correlated to the obstruction of Q diffusion in the presence of B; is it not possible that the same mechanism operates in the structural alloys too? I am also led to think that the beneficial effect of B in austentic stainless steels which contain some carbon, may also be of a similar kind.

Finally the kinetics of oxidation of metal surfaces is a complex process even in simple cases [27, 28]. Our current understanding of the oxidation of a binary alloy such as Ni-Cr is so inadequate that we cannot even begin to make judgments about the oxidation kinetics of multicomponent engineering alloys [29]. For example, a Cr_2O_3 layer on chromium may be tenacious but in a Ni-Cr alloy the oxide scale can contain two or more layers of different compositions (because of kinetic considerations [27]) and therefore, it may be more susceptible to cracking due to lattice mismatch, thermal stresses and deformation.

Acknowledgements – This research was supported by the Air Force Office of Scientific Research AFOSR-80-0008 under the supervision of Dr A. H. Rosenstein. Partial support was received from the National Science Foundation through the Materials Science Center at Cornell University. It is a pleasure to acknowledge helpful discussions with Professors H. H. Johnson and G. R. Odette. I am grateful to the reviewer for his comments which led to Section 7 and to S. Floreen for sharing his ideas and experience.

REFERENCES

1. K. Sadananda and P. Shahinian, *Mater. Sci. Engng* **43**, 153–168 (1980).
2. R. L. Stegman and P. Shahinian, *Am. Soc. Test. Mater. Spec. Tech. Publ.* **459**, 42–58 (1969).
3. H. H. Smith, P. Shahinian and M. R. Achter, *Trans. T.M.S.-A.I.M.E.* **245**, 947–953 (1969).
4. D. A. Woodford, *Metall. Trans.* **12A**, 299–308 (1981).
5. R. H. Bricknell and D. A. Woodford, Gen. Elec. Corporate R & D, Schenectady, NY, Report No. 80CRD164 (1980).
6. D. A. Woodford and R. H. Bricknell, Gen. Elec. Corporate R&D, Schenectady, NY, Report No. 80CRD259 (1980).
7. H. D. Solomon and L. C. Coffin Jr, *Am. Soc. Test. Mater. Spec. Tech. Publ.* **520**, 112 (1972).
8. R. Raj and M. F. Ashby, *Acta metall.* **23**, 653–666 (1975).
9. R. Raj, H. M. Shih and H. H. Johnson, *Scripta metall* **11**, 839–842 (1977).
10. R. Raj, *Acta. metall.* **26**, 995–1006 (1978).
11. D. R. Gaskell, *Introduction to Metallurgical Thermodynamics*, p. 497. McGraw Hill, New York (1973).
12. A. D. Kulkarni and W. L. Worrell, *Metall. Trans. A* **3**, 2363–2370 (1972).
13. JANAF Thermochemical Tables, 1975 Supplement National Bureau of Standards, Washington, DC., *J. Phys. Chem. Ref. Data* **4**, 92 (1975).
14. K. K. Kelley, F. S. Boericke, G. F. Moore, E. H. Huffman and W. M. Bangert, U.S. Bur. Mines Tech. Paper, 1949, Vol. 662 (1949).
15. M. Small and E. Ryba, *Metall. Trans. A* **12A**, 1389–1396 (1981).

16. R. C. Evans, *An Introduction to Crystal Chemistry*, p. 69. Cambridge University Press, Cambridge (1966).
17. S. H. Maron and D. Turnbull, *J. Am. Chem. Soc.* **64**, 2195 (1942).
18. D. S. Tsiklis, L. R. Linshits and S. S. Tsimmerman, Abstracts of All-Union Thermophysical Conference on Properties of Substances at High Temperatures, Odessa, 1970 (referenced in G. R. Odette and S. S. Vagarali, *Analysis of Hydrogen Attack on Pressure Vessel Steels*, Report DOE Contract No. ET-78-S-01-3153, University of California, Santa Bargara, Sept. 1980).
19. W. E. Deming and L. E. Shupe, *Phys. Rev.* **38**, 2245 (1931).
20. A. S. Leah, *Thermodynamic Functions of Gases*, edited by F. Din, Vol. 1, p. 135 (1962).
21. R. G. Fleck, D. M. R. Taplin and C. J. Beevers, *Acta metall.* **23**, 415 (1975).
22. N. G. Needham and T. Galdman, *Metal Sci.* **14**, 64–72 (1980).
23. W. Johnson and P. B. Mellor, *Plasticity for Mechanical Engineers*, p. 148. Vern Nostrand, New York (1962).
24. H. M. Shih and H. H. Johnson, *Acta Metall.* **30**, 537 (1982).
25. J. K. Tien and J. M. Davidson, *Adv. Corr. Sci. Tech.* **7**, 1–51 (1980).
26. S. Floren, private communication.
27. C. Wagner, *Z. Electrochem.* **63**, 772 (1959).
28. R. A. Rapp, *Corrosion* **21**, 382–401 (1965).
29. S. T. Wlodek, *Trans. metall. Soc. A.I.M.E.* **230**, 1078–1090 (1964).

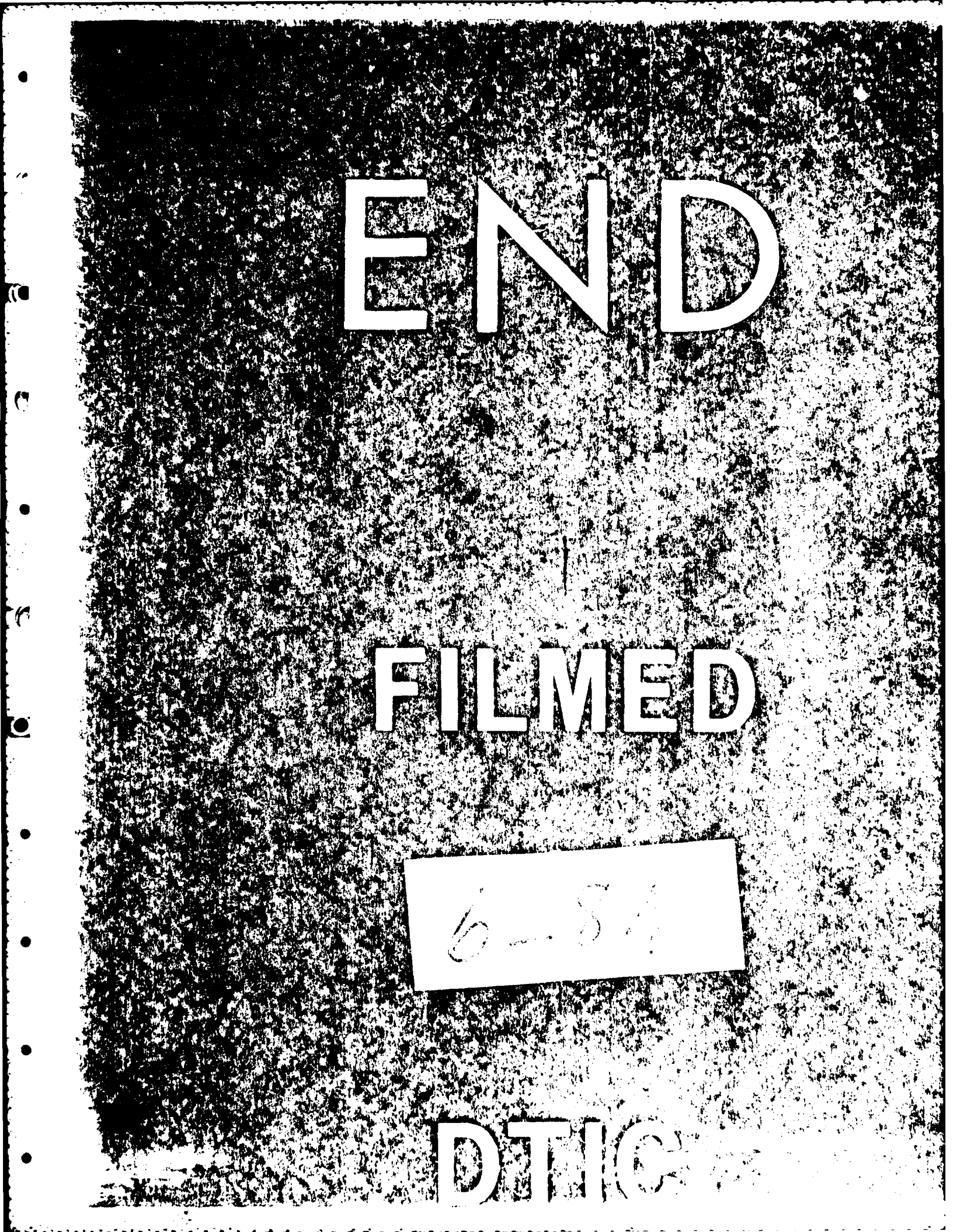
END
FILMED
DTIC